Qeios

Lunar Rover Grand Prix Sequence in Apollo XVI Footage: Behavior of Lunar Dust and Known Dimensions of Involved Objects

ABSTRACT

This manuscript develops and integrates the previous studies "***Analytical Methods for Tracking Bodies Motions on the Lunar Surface in Apollo XVI Footage***" https://doi.org/10.32388/IA8MXE, "***Ballistic motion of dust particles in the "Collecting the Big Muley lunar rock sequence of the Apollo XVI Footage"*** https://doi.org/10.32388/COXHKG.2, "***Falling Objects and Dust Particles' Motion in the Collecting Lunar Rock on the Buster Crater sequence of the Apollo XVI Footage***" https://doi.org/10.32388/RFR2D5, in order to introduce a robust analytical method to trace and analyze the movement of dust shot during the Apollo XVI mission on the lunar surface. By employing both 2D and 3D analysis techniques, we aim to provide a detailed comparison of the observed kinematic events against theoretical models.

The paper extends a previous work focused on the kinematics of lunar dust utilizing footage from the Apollo XVI mission "*Ballistic motion of dust particles in the Lunar Roving Vehicle dust trails*" published in 2012 in the American Journal of Physics by Mihaly Horanyi and Hsiang-Wen Hsu: https://www.researchgate.net/publication/258468670 [Ann. 1 – Ann. 2].

In this further analysis, the famous sequence of the LRV "Grand Prix", a performance test recorded by the Maurer DAC Camera at the end of EVA 1, is tracked and analyzed with the professional tools adopted in the other sections of the study. The behavior of the so-called "Roster Tails", the dust trails raised by the wheels of the LR during its march, is compared with the motion models related to the lunar environment. A jump of the vehicle that keeps it in free fall for about 1 second is analyzed and starting from the fit tests of the detected data, conclusions are drawn about the characteristics of the moving objects and about the environment in which the sequence takes place.

Disclaimer:

We do not in any way question the fact that humans landed on the Moon. Our aim is to explore potential discrepancies in the footage, which could be attributed to artifacts, possible errors in the original footage conversion or transformation, calculation errors, or incomplete data on the technical parameters of the mission.

Keywords:

Apollo 16, Lunar dust ballistic motion, Lunar Rover Grand Prix, Apollo footage.

SECTION E
Grand Prix

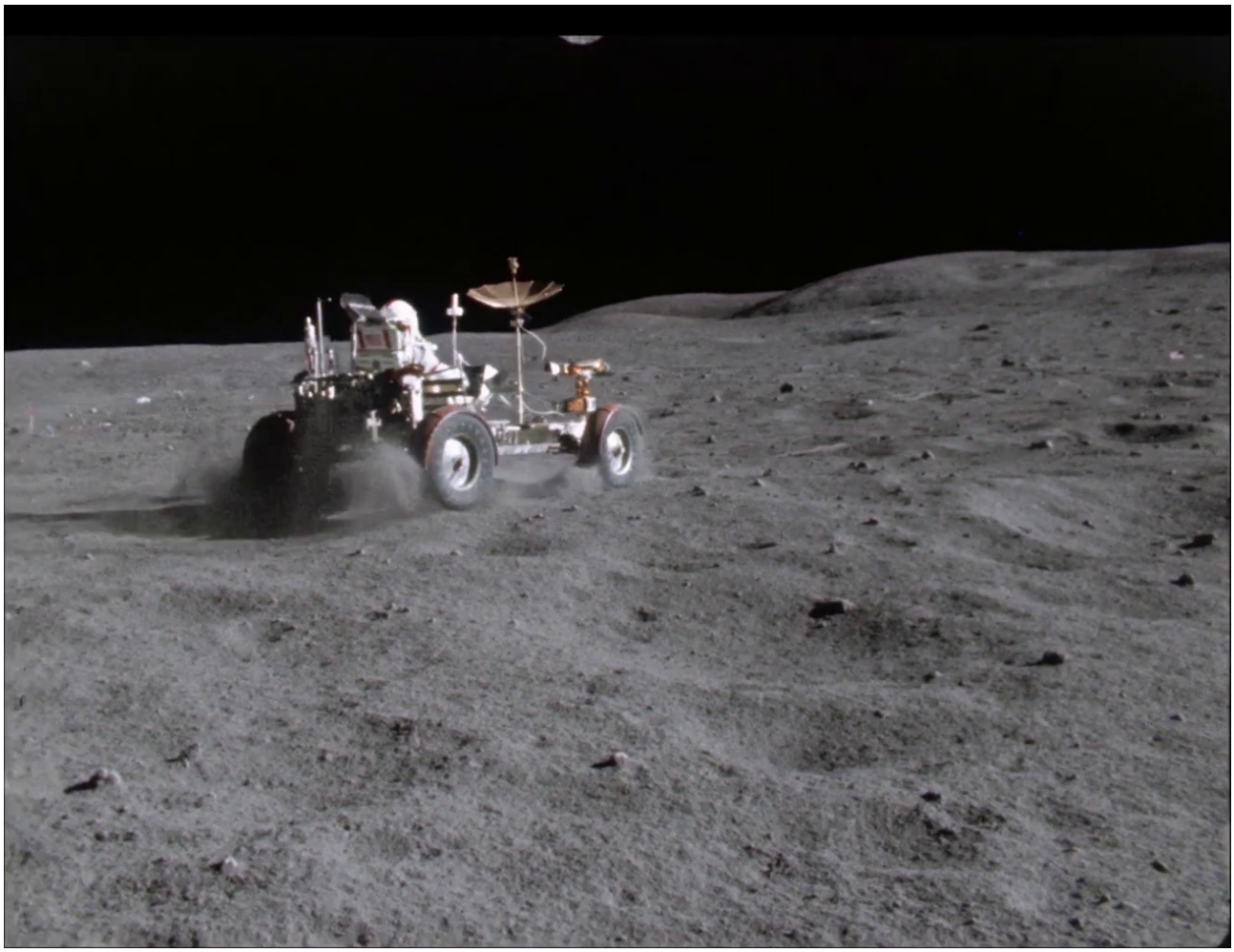

Figure E1 - LR Grand Prix, EVA 1, Frame HD released in 2019 on the Facebook page apolloflightjournal [1]

E.1.1 Testing of the LRV

Back from the Buster Crater (Station 2), at the end of EVA 1, John Watts Young prepares to perform a performance test of the Boing-built Lunar Rover Vehicle at the ALSEP site. The sequence will be shot by Charles Duke with the Maurer Data Acquisition Camera on 16mm film. Therefore, it will not be broadcast live on TV worldwide, but following the mission, once developed and released in the context of the "Nothing so hidden" film, it will become one of the most popular video documents of all the Apollo missions. This film has been re-photographed several times and uploaded online in digital format. The latest HD version was published on the 18th of March 2019 on Facebook and on the 8th of July 2019 on YouTube.

Having dedicated the introduction of this study to the two clips of this sequence studied by the Colorado Center for Lunar Dust and Atmospheric Studies, NASA Lunar Science Institute, it's right to close this work by returning to analyze the same images in light of the investigative tools that we have previously identified.

---

[1] *https://www.facebook.com/apolloflightjournal/videos/315560545801914 NASA, 18th march 2019 [Ann. E1]*

E.1. 2 Chronicle [2]

[Charlie has taken off his Hasselblad, so it won't get in the way while he uses the 16-mm camera. The Data Acquisition Camera (DAC) has a bracket mounted on the back which would allow Charlie to mount the camera on his Remote-Control Unit (RCU). Apollo 13 training photo KSC-70PC-18 shows Fred Haise with a DAC mounted on his RCU. The character of the 16-mm film that Charlie shot - reasonably steady with John well centered - suggests that Charlie held the camera in his hands.]
124:54:45 Duke: Okay. Now let me see. (As per LMP-26), you're suppose to drive 45 degrees to the Sun. Okay?
124:54:51 Young: Yep.
124:54:52 Duke: Okay. Let me get the 16(-mm camera) off.
124:54:55 Young: I'll do it from there up towards this way. Okay?
124:54:58 Duke: Wait a minute. Okay, which way you gonna drive? From here, this way?
124:55:02 Young: Going over...
124:55:03 Duke: Towards Stone (Mountain)?
124:55:04 Young: You see where that white thing is?
124:55:05 Duke: Yeah.
124:55:06 Young: I'll go over there toward a rock and drive up this way. Okay?
124:55:09 Duke: Okay. Well, wait. Why don't you just drive towards the LM. Let me move out here, and you just drive towards the LM, turn around, and then drive towards Stone.
124:55:17 Young: Okay.
124:55:18 Duke: Okay?
124:55:19 Young: Okay.
124:55:20 Duke: Let me get the camera. Let me get it set here now. It's 24 (frames per second). Gonna be using the trigger, so (as per the notation at the top of LMP-26) it's 24 (pause) and f/8 at 250(th of a second).
124:55:39 Young: Hey, that LM makes a nice-looking house. (Pause)
124:55:50 England: Especially since it's about the only one there.
124:55:56 Young: Yeah.
124:55:59 Duke: You're right, Tony. It ain't nothing much up here but a lot of rocks.
124:56:03 Young: Hope the (LM) door opens, Charlie.
124:56:05 Duke: Huh? What?
124:56:07 Young: I said, I hope the door opens.
124:56:08 Duke: It'll open. (Garbled) close it. (Grunting) This thing is stuck. I can't get it up. Let me move out. Okay. To start, I'm suppose to be about 50 meters or so from you.
124:56:28 Young: Okay, Charlie. And what I'll do (as per CDR-36) is drive from A to B, standing start, max velocity readout. And (pause) then do some...I'm not going to do much steering control around here, other than to avoid regular craters. I'm going to have to do that anyway.
124:56:51 Duke: Yeah. Okay. I'm ready.
124:56:53 Young: And I'm not going to brake it, to amount to anything.
16-mm film clip (2 min 20 sec; 75 Mb) by Ken Glover from material provided courtesy of Mark Gray, including synched audio. Mac users may need VLC (free download). Journal contributor Maksim Kakitsev has created a stabilized version of various Apollo 16 film clips, including the Grand Prix.
124:56:58 Duke: DAC's on; Mark. (Pause) That max acceleration?!
124:57:06 Young: No. (Pause)
124:57:10 Duke: Man, you are really bouncing! (Pause)
124:57:14 England: Is he on the ground at all...
124:57:16 Young: Okay; that's 10 kilometers (per hour). (Hearing Tony) Huh?
124:57:20 Duke: (To Tony) He's got about two wheels on the ground. There's a big rooster tail out of all four wheels. And as he turns, he skids. The back-end breaks loose just like on snow. Come on back, John. (Pause) And the DAC is running. Man, I'll tell you, Indy (meaning the Indianapolis 500)'s never seen a driver like this. (Pause) Okay, when he hits the craters and starts bouncing is when he gets his rooster tail. He makes sharp turns. Hey, that was a good stop. Those wheels just locked.

---

[2] *https://www.hq.nasa.gov/alsj/a16/a16.trvlm1.html Apollo 16 Lunar Surface Journal Corrected Transcript and Commentary by Eric M. Jones. Revised 5 March 2016.*

124:58:03 Duke: Mark, (the camera's) off.
124:58:05 England: Okay.
[NASA photo S72-37002 is a frame from the 16-mm movie. It shows John driving in an easterly direction, toward the LM, with Smoky Mountain on the horizon on the right side of the picture. We can see the dust being thrown up by the wheels and can also see that the fenders are effective in keeping that dust from being thrown onto the vehicle. Not counting the turn John made before coming back on the return leg, John drove about 25 seconds in each direction. His average speed would have been less than 10 km/hr, so the distance he drove in each direction would have been less than 70 meters.]
124:58:06 Young: Okay, you want to do it one more time?
124:58:07 England: Had about a minute and 5 seconds that time.
124:58:08 Duke: Yeah, (lost under Tony).
16-mm Film Clip (2.3Mb; mov) by Gordon Roxburgh
124:58:10 Duke: Okay. Mark; on. (Pause) Okay. You could have gone the other way, but go ahead. There's the big craters there, though, aren't they?
124:58:19 Young: Yeah. I don't want to run into those holes.
124:58:24 Duke: They want 4 minutes' worth, John. That was a minute and five (seconds). Maybe you can do it twice more.
124:58:30 Young: (Lecturing) Charlie!
124:58:31 Duke: Okay. Turn sharp.
124:58:34 Young: (Laughing) I have no desire to turn sharp. (Charlie laughs, too.) Okay, here's a sharpie.
124:58:39 Duke: Hey, that's great! (Pause) Man, those things...When those wheels really dig in, John...When you turn is when you get the rooster tail.
124:58:51 England: Charlie?
124:58:52 Duke: The suspension system on that thing is fantastic!
124:58:54 England: That sounds good. We sound like we probably got enough of the Grand Prix. We're willing to let you go on from here. Call that a (complete) Grand Prix.
124:59:03 Duke: Okay. (Pause) Man, that was all four wheels off the ground, there. Okay. Max stop.
124:59:12 Young: Okay. I don't want to do that.
124:59:13 Duke: Okay. Excuse me.
124:59:16 Young: They say that's a no-no.
124:59:22 Duke: Okay, DAC off; Mark. Okay, John. DAC's off.

E.1.3 Basic Technical Data

The Lunar Surface Journal, in accordance with what was stated directly by Charles Duke in the audio recorded during the mission, offers the following basic technical data relating to the shooting.

Film type: *16-mm film*
Framerate: *24 frames per second*
Lens aperture: *f/8*
Initial distance of the subject from the lens: *50 meters*
Average speed of the LRV: *approximately 10 km/h*
Maximum distance traveled in the same direction: *approximately 70 metres.*

A very important technical data is stated in the Apollo 16 Index of Photographs and Film Strips [3], where it appears that the sequence was shot with a 10mm lens. In fact, the Swiss production company Kern [4] had supplied 4 lenses with different focal lengths for the Maurer DAC (including

---

[3] *https://www.hq.nasa.gov/wp-content/uploads/static/history/alsj/a16/a16.photidx.pdf Apollo 16 Index of 70 mm Photoraphs and 16 mm Film Strips pag 19, Manned Spacecraft Center Houston, Texas - November 1972* [*Ann. 3*]
[4] *https://www.kern-aarau.ch/fileadmin/user_upload/Aldo/Optik/Haefliger_Kameras_Optik_Objektive_NASA.pdf* [*Ann. E2*] *Photographica Cabinett The Magazine for Collector, n 67, 2016, page 8, Rolf Häfliger, Kern Aarau CH*

an 18 mm lens), but these supplies were intended for the Maurer cameras [5] of the Command Module and not for the models – although similar – used during the EVAs.

To verify these data, we help ourselves with simple geometric considerations about the images and the optics that generated them. The frame shown in Figure E2 is extracted from the HD video released by NASA in 2019 [5]. This is one of the frames from the beginning of the sequence, taken when the LR is still stopped and its distance from the lens should be around 50 m. The frame is made homographic with the image printed on the 16mm sensor (10.26 mm X 7.49 mm), with an aspect ratio of 1.37.

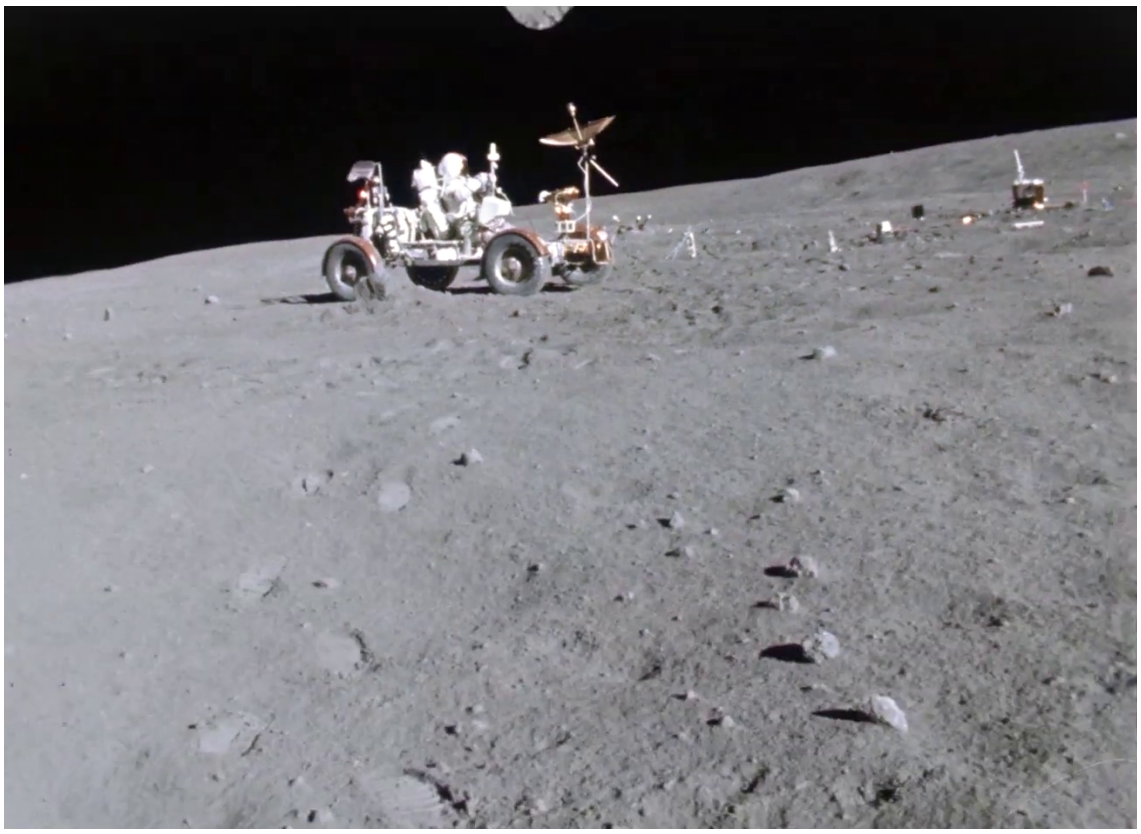

Figure E2 – (frame 1) Lunar Rover Grand Prix, EVA 1, initial frame, @apolloflightjournal Facebook page 2019 [1]

Considering that $\text{Distance} = \frac{Focal * dWheel_{moon}}{dWheel_{film}} = \frac{10\ mm\ X\ 818\ mm}{0.6\ mm} = 13.633$ mm = 13.63 m

the technical data do not seem to confirm that the LR was at the declared distance.

The figure below represents the extract of a frame that is located approximately in the middle of the sequence released on the official Facebook page @apolloflightjournal on 18th March 2019, between the first and second laps of the Luna Rover Grand Prix. The image was compared with identical frames of previous digital copies of the film imprinted by the Maurer DAC (in particular with

[5] https://tothemoon.ser.asu.edu/files/apollo/apollo_16_lunar_photography.pdf *Apollo 16 Lunar Photography (Data User Note) page 3. NASA - National Space Science Data Center, Goddard Space Flight Center, National Aeronautics and Space Administration - Greenbelt, Maryland, May 1973*

Apollo 16 Journey to Descartes, complete TV and onboard film © 2005 Spacecraft Film, courtesy NASA). In the new release, the image field is wider than in previous versions, but some pixels in the upper part of the image are cut off. To guarantee greater integrity of the original image, the same frame was superimposed with the two versions.

Figure E3 – (frame 2) Lunar Rover Grand Prix, frame extracted from the sequence published in 2019 at second 1:29

The Rover is significantly closer, a strip of ground emerges in the field near the lens enough to allow the shadow of Duke's helmet to enter the frame. The LR antenna touches the top edge of the image, a sign that Charles Duke tends to tilt the camera further downwards. In this frame, the front wheel of the Rover has a dimension of 1.2 mm on the sensor, which means that the distance from the lens is:

$$D = \frac{10\ mm\ X\ 818\ mm}{1.2\ mm} = 6.82\ \text{m}$$

E.1.4 Geometric aberration of images

As we saw in the introduction to this study, the focal length of the lens used to shoot the scene of the Grand Prix (10 mm), considered the 16 mm sensor, entails an equivalent focal length:

$$Fe = F \cdot \frac{D_S}{D} = 10\ x\ 43.3\ /\ 12.70 = 34.1\ mm$$

Since it is Fe close to the focal length values for which the aberration is considered negligible, in this case, no image correction procedure is implemented.

E.1.5 Study of Shadows

The Lunar Surface Journal publishes the solar inclination angle of each of the 6 Apollo missions [6]. In Apollo 16 - EVA 1 the sun rises up about half a degree per hour starting from 22.2° and reaching 25,7° seven hours later. During the Grand Prix, the inclination of the sun's rays must have been around 25.2°. This means that by considering Charles Duke's height of about 2 meters, we expect the shadow to be long:

$$\text{Length(Shadow)} = \frac{2.00\ \text{m}}{\tan(25.2)} = 4.25\ \text{m}$$

This data corresponds to what is documented by the images taken with CTV and sent live to the global television circuit. Figure E4 represents the extract of a frame taken in the same area in which the Grand Prix takes place, during the preparation of the Apollo Lunar Equipment Surface Experiments Package (ALSEP), in EVA 1, 121 hours and 52 minutes after the start of the mission, that is approximately 3 hours before the Grand Prix sequence shot with the 16mm Maurer DAC film camera. It can be noted that Charles Duke's shadow is very long. Its measurement is detected with Adobe Photoshop according to the technique used several times in the previous sections of this study.

The astronaut, slightly bent on his legs, reaches a height of 1.91 m. Given the angle of inclination of the sun's rays at this moment, according to the Lunar Surface Journal was about 23.7°, its shadow is expected to measure:

$$\text{Length(Shadow)} = \frac{1.91\ \text{m}}{\tan(23.7°)} = 4.35\ \text{m}$$

The measurement carried out returns the result of 4.28 m, sufficiently consistent with what was defined theoretically.

Hasselblad cameras document a significantly different situation. Figure E5 represents the photo AS16-114-18388 published on the *Apollo 16 Images Library* [7] and taken once again in the ALSEP area 122 hours and 46 minutes after the mission started, approximately 1 hour from the previous CTV shot and 2 hours before the Grand Prix sequence. In this case, the astronaut's shadow (John Young) appears much shorter. At that moment the sun was tilted approximately 24.2° and the shadow should have been approximately 434 cm long. The measurement result presented in Figure E5 (shadow length of 2.4 m) can only be obtained by assuming that the sun was much higher above the lunar horizon. The inclination of the sun's rays had to be at least:

$$\alpha = Arctang\left(\frac{1.95\ m}{2.40\ m}\right) = 39.0°$$

---

[6] https://www.hq.nasa.gov/alsj/alsj-sunangles.html *Apollo Lunar Surface Journal, NASA, Compiled by Brian W. Lawrence, by Eric M. Jones 1995-2017. Last revised 11 October 2005.*

[7] https://history.nasa.gov/wp-content/uploads/static/history/alsj/a16/AS16-114-18388HR.jpg *Apollo 16 Images Library, NASA, by Eric M. Jones 1996-2017. Last revised 16 March 2019. [Ann. E3]*

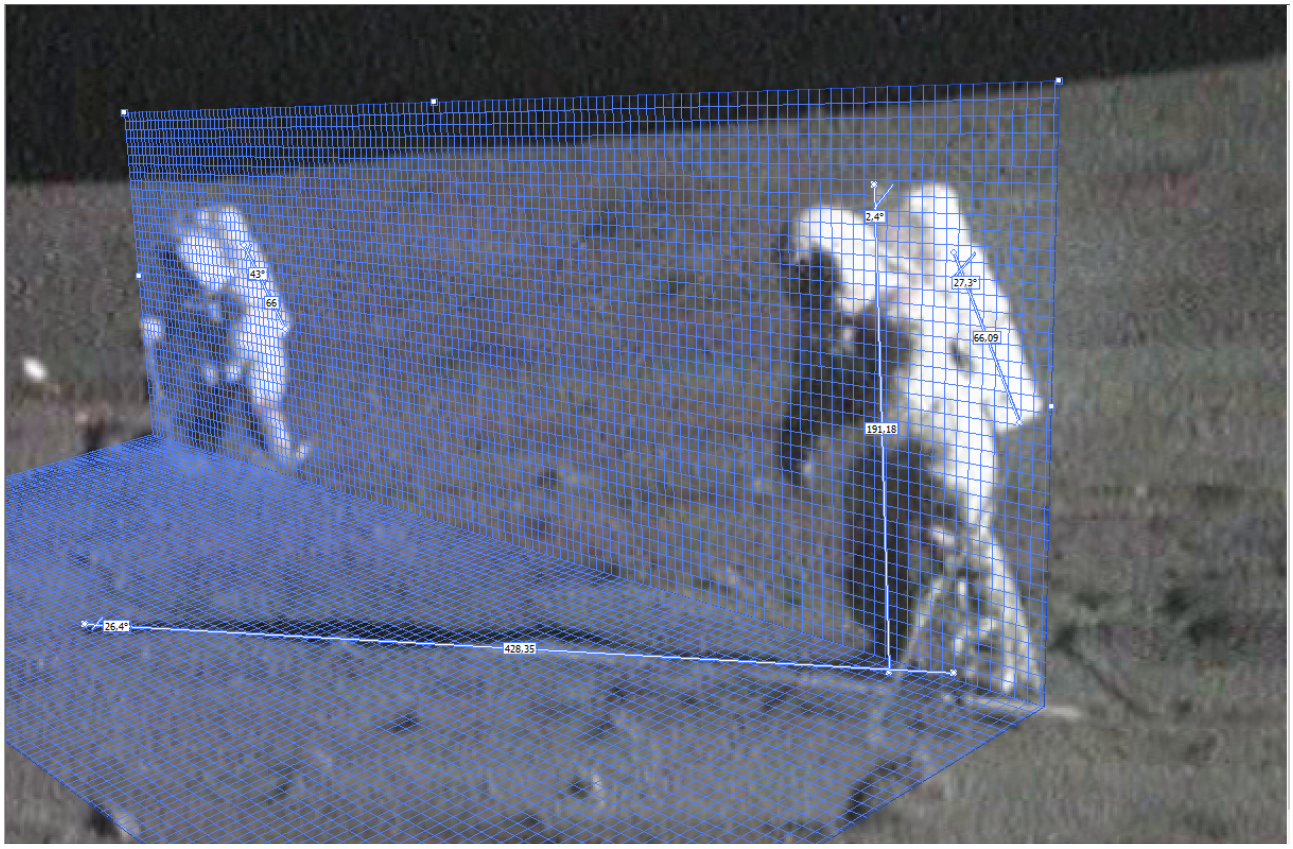

Figure E4 – ALSEP deployment, 121:52 mission time, length of Charles Duke's shadow

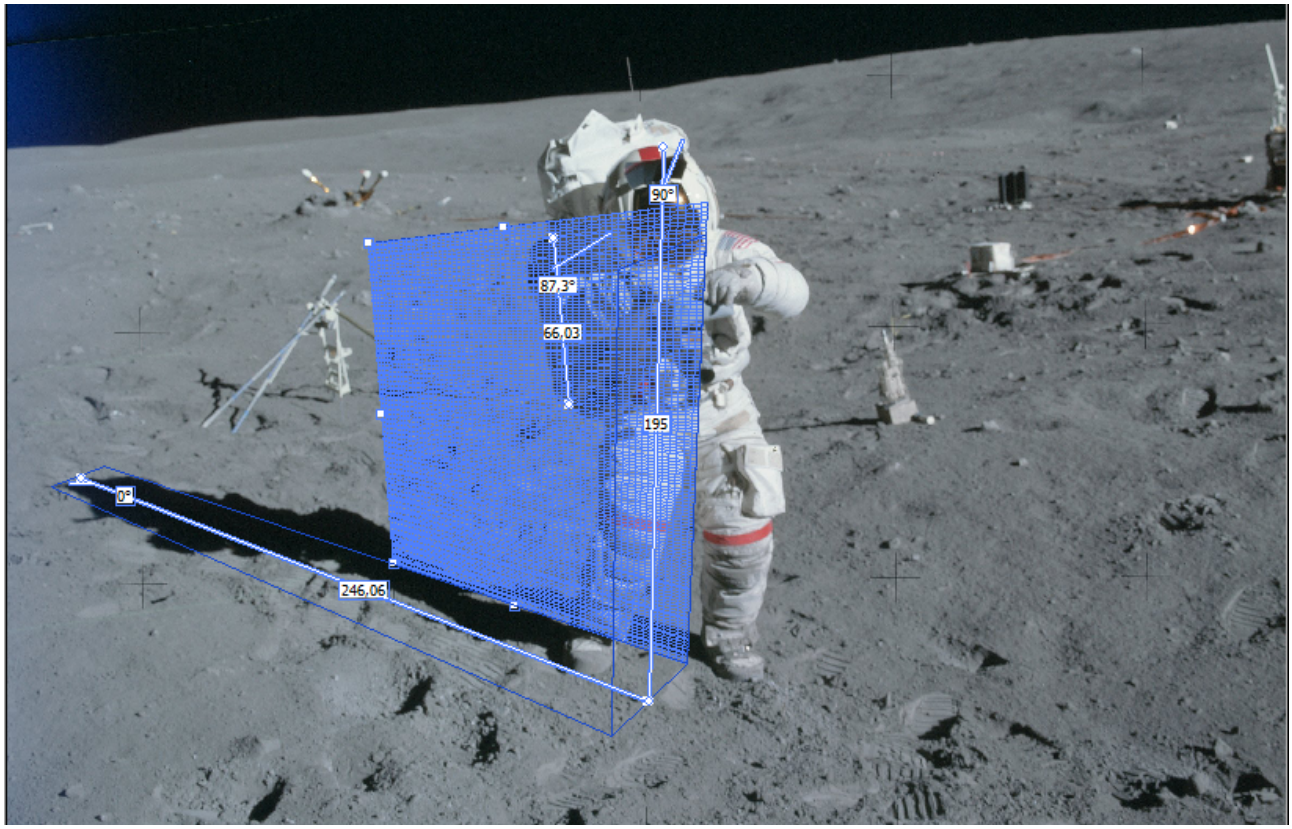

Figure E5 – EVA 1, 122:46 mission time, Hasselblad 70 mm photo, length of John Young's shadow

We can verify that the shadows taken with the Maurer DAC camera also have the same inclination, measuring the stones in the frame of Figure E2: the length of their shadow confirms the data obtained from the Hasselblad photos.

$$\alpha = Arctang\left(\frac{158.57\ mm}{195.57\ mm}\right) = 39.0°$$

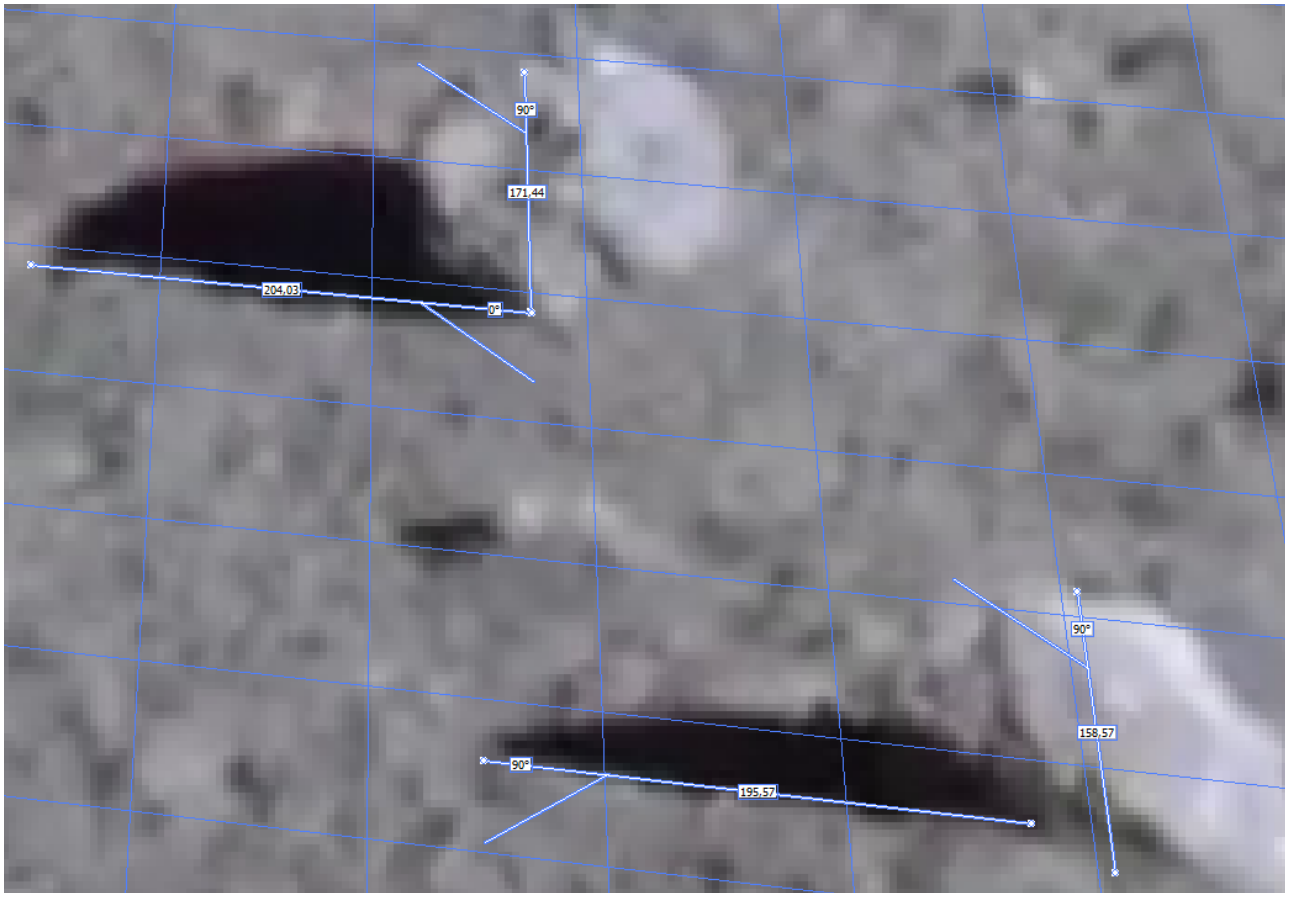

Figure E6 - Lunar Rover Grand Prix, EVA 1, initial frame: study of shadows.

An inclination that seems incompatible with the scientific data available on the lunar environment that should have hosted the ALSEP set-up operations when the operations would have taken place. This could be due to errors in our methodology, unaccounted-for factors such as lens distortion, or environmental conditions. If any errors in our calculations or methodology are identified, we would be grateful for feedback.

E.1.6 Position of the Maurer Data Acquisition Camera

One of the fundamental elements for identifying the correct optical system used for the Lunar Rover Grand Prix film is the definition of the position of the Cine-Camera with which the shot itself was carried out.

The *Lunar Surface Journal* hypothesis reported at the beginning of this chapter is that the Camera was attached to the ring prepared on the space suit, about 1.60 m above the ground, similar to what is reproduced in Figure E7.

Figure E7 - Apollo 13 LMP Fred Wallace Haise practices with the Maurer DAC during an EVA simulation.[8]

Generally speaking, this was the position of the Hasselblad and also of the Maurer cameras during the Apollo missions, as confirmed by many NASA sources, and in particular by Gary H. Kitmacher and Steve Garber, in the article " *Astronaut Still Photography During Apollo* ", [9] which states that "*the most crucial training was in pointing the camera which was attached to their chest control packs for the suit's environmental control system. The astronaut would point his body in order to*

[8] https://www.nasa.gov/feature/50-years-ago-apollo-13-launch-date-reset *NASA, Page Last Updated: Jan 13th, 2020, NASA Official: Brian Dunbar*

[9] https://history.nasa.gov/wp-content/uploads/static/history/apollo_photo.html *Gary H. Kitmacher, Author Steve Garber, NASA History Web Curator "Astronaut Still Photography During Apollo" National Aeronautics and Space Administration Official Website*

aim the cameras". The *Lunar Surface Journal* also adds another detail, suggesting that Duke held Maurer in his hands.

To facilitate shooting, the DAC also had a ring viewfinder. The light and dark concentric circular rings, superimposed on the frame, helped the operator determine the angular field of view. It was attached to the camera via its sleigh which slid in a rail on the top side. However, it is clear that this tool could not easily be used when the camera was fixed to the suit, lower than the helmet. In that position, compatible with wide-angle lenses, the conditions described in the article by Gary H. Kitmacher and Steve Garber probably occurred, that is "*the astronaut would point his body in order to aim the cameras*".

Given the convergence of several official sources, we assume, at least preliminarily, that the position of the camera was the one declared on LSJ.

E.1.7 Identification of the optical system

Let's consider the different vertical field angles relating to the two frames of the Grand Prix sequence that we intend to analyze taking into account the two Kern optics supplied for the Maurer DAC.

$$\alpha_v = 2 * \arctan\left(\frac{hsensor}{2*focal}\right) = 2 * \arctan\left(\frac{7.49\ mm}{2*focal}\right)$$

With a 10 mm focal length we have $\alpha_v = 41.06°$. These values agree with those declared in the *Apollo 16 Lunar Photography (Data User Note)* published by NASA's National Space Science Data Center in May 1973 [5], considering the approximation of the sensor measurements present in the technical document (the 16 mm format is indicated as 10 X 8 mm instead of 10.26 X 7.49).

Having assumed the position of the Camera at 1.60 m in height as described in E.1.6, we note an inclination of it in both frames. The center of the image is actually lower than the height of the camera we assumed and also than any other position it could have assumed on the body or in the hands of the operator.

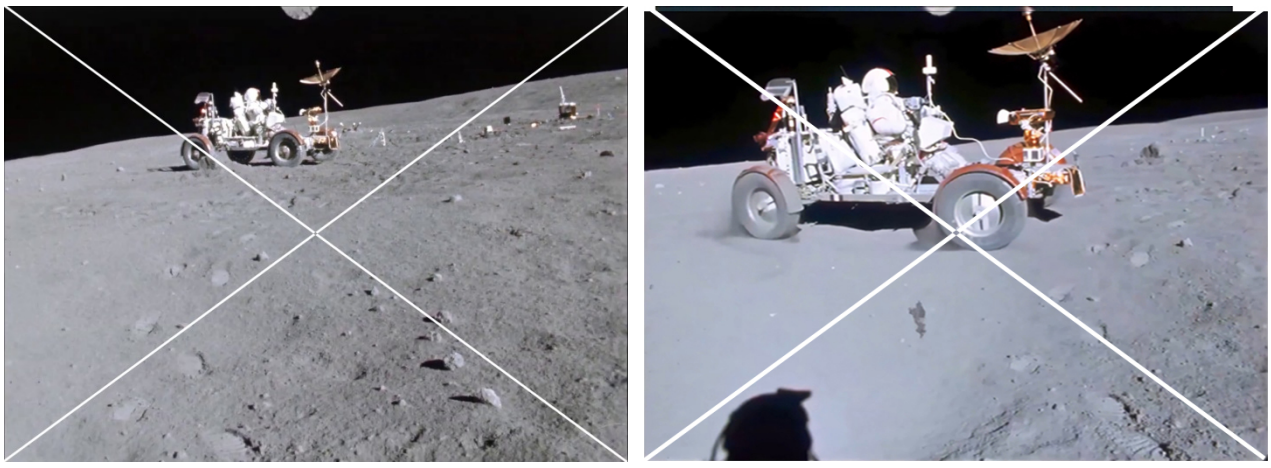

Figure E8 - Lunar Rover Grand Prix, center of the analyzed images

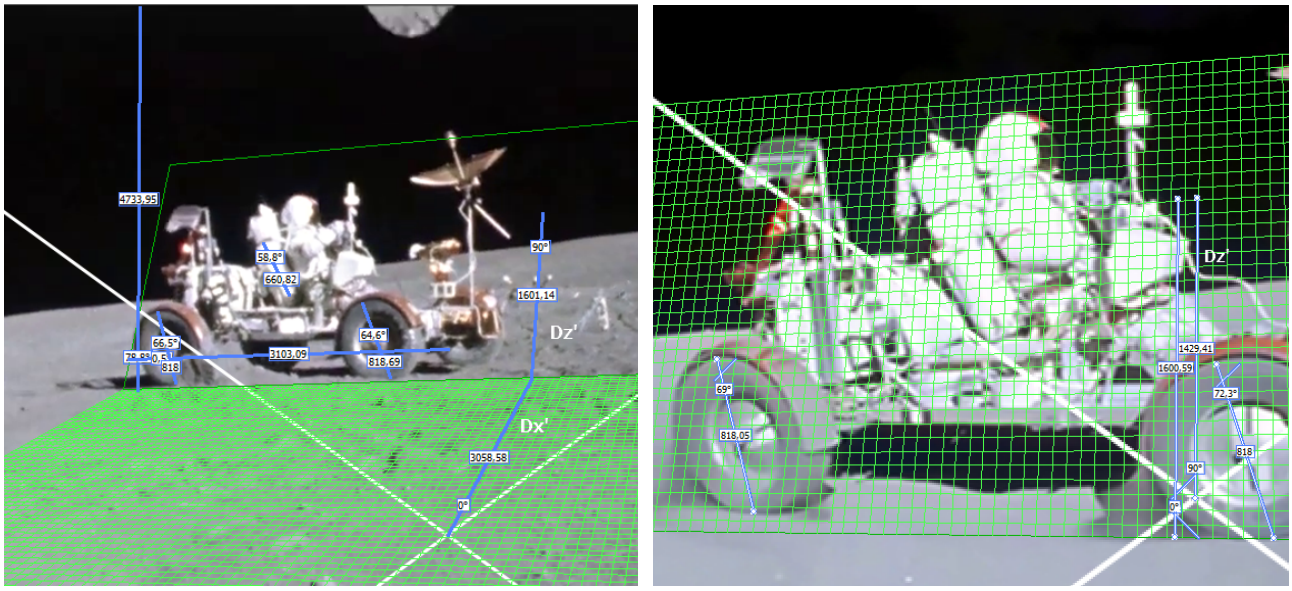

Figure E9 – LR Grand Prix, distance of the image center with respect to the height of the optical axis of 1600 mm

In frame 1 the center of the image corresponds to a point on the lunar surface, located at a distance $D_{x'}$ = 3.06 m from the subject.

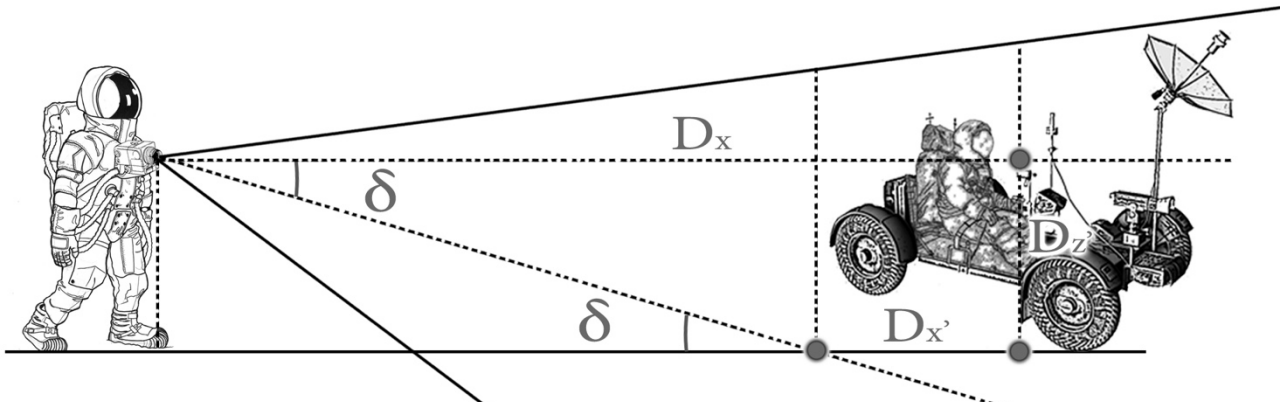

Figure E10 - Lunar Rover Grand Prix, EVA 1, Maurer DAC tilt in Frame 1

As highlighted in Figure E10 in this first frame, the angle of inclination of the camera with respect to the ground line can be calculated with the formula:

$$\delta = arctan\left(\frac{D_{z\prime}}{D_x - D_{x\prime}}\right)$$

In Frame 1 $D_x = \sqrt{13.63^2 + 1.60^2} = 13.54\ m$ e $\delta = arctan\left(\frac{1.60}{10.48}\right) = 8.68°$

In frame 2 the center of the image insists on the subject, so as is clear from the following Figure E11 the inclination angle of the camera can be obtained with:

$$\delta = arctang\left(\frac{D_z}{D_x}\right)$$

In the second frame, the inclination is therefore $\delta = 12.17°$. As regards the upper limit of the frame (Figure E11) we can easily calculate the highest point that can be framed by the cine camera on the vertical of the LR with respect to the ground line.

$P_{max} = 1.60\ m + D_x * \tan\left(\frac{\alpha}{2} - \delta\right)$ or:

Frame 1, Focal length 10 mm: $P_{max} = 1.60\ m + 13.54\ m * \tan(11.85°) = 4.44\ m$
Frame 2, Focal length 10 mm: $P_{max} = 1.60\ m + 6.63\ m * \tan(8.36°) = 2.57\ m$

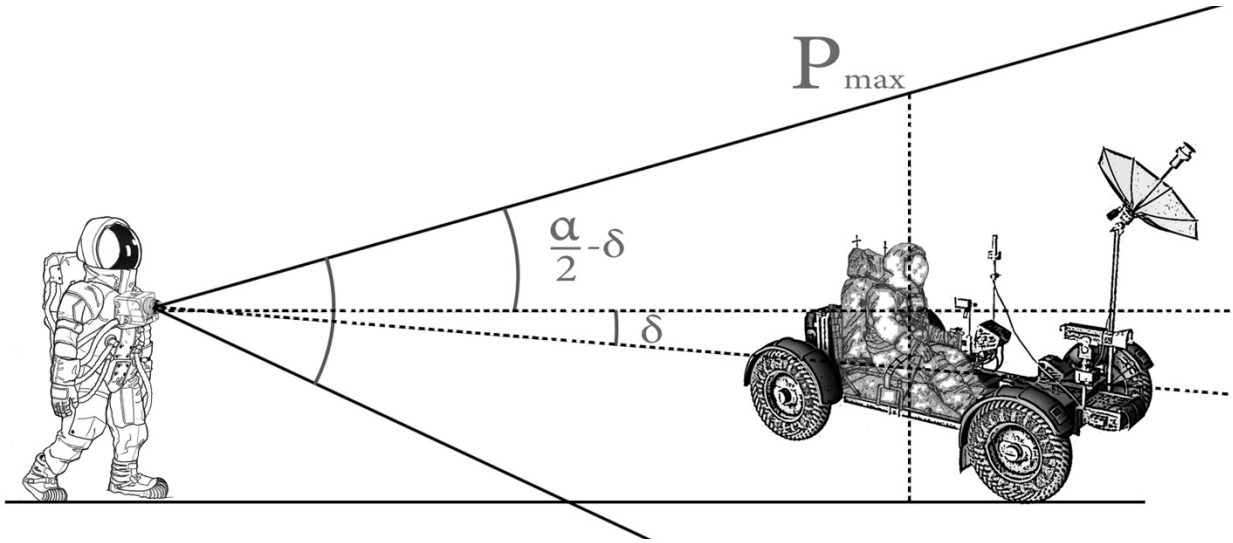

Figure E11 - Lunar Rover Grand Prix, EVA 1, the highest point that can be framed on the vertical of the LR

The closest point that can be framed to the ground is found in:

$P_{min} = Height_{dac} * \tan(\beta)$ with $\beta = 90° - \left(\frac{\alpha}{2}\right) - \delta$

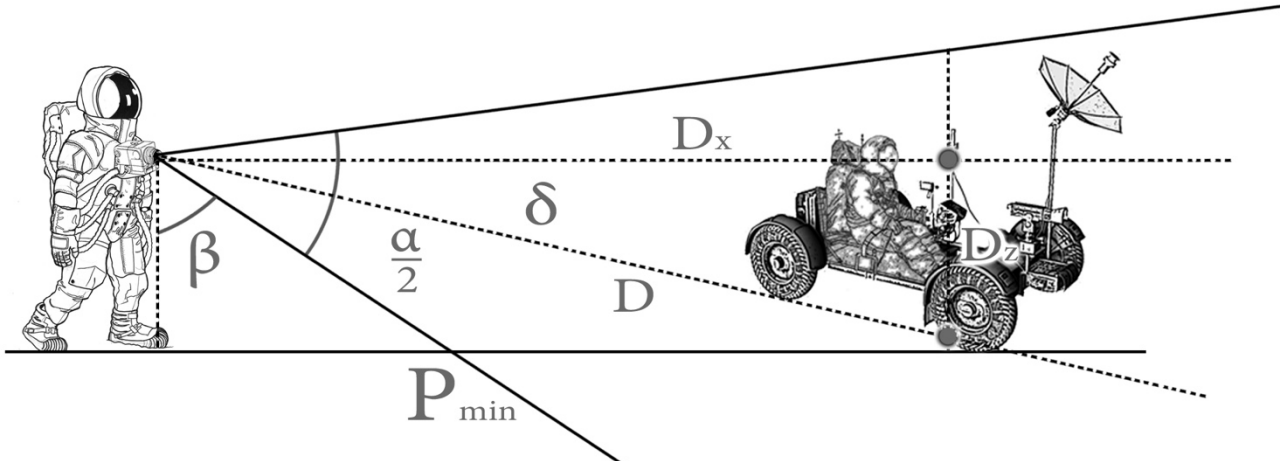

Figure E12 - Lunar Rover Grand Prix, EVA 1, Maurer DAC field angle and camera inclination

That is to say:
Frame 1, with 10 mm focal length: $P_{min} = 1.60\ m * \tan(60.79°) = 2.86\ m$
Frame 2, with 10 mm focal length: $P_{min} = 1.60\ m * \tan(57.30°) = 2.49\ m$

Given the inclination of the sun's rays calculated in E.1.5 according to the scientific data presented by *Lunar Surface Journal*, Duke's shadow should be 4.25 m long. Having detected on Frame 2 the projection angle of the shadow with respect to the optical axis, with the help of the Vanishing Point Filter of Adobe PS CS6 (as can be seen in Figure E13 it corresponds to 25°), it should come into frame up to:

$$Length\ of\ visible\ shadow = 4.25 - \frac{P_{min}}{\cos(25°)}$$

That is to say:
Frame 1, with 10 mm focal length: 1.09 m
Frame 2, with 10 mm focal length: 1.50 m

However, by carrying out the necessary measurements on Frame 2, as illustrated in Figure E13, the actual length of the visible shadow is found to be 0.35 m. This demonstrates that the P_{min} points identified in the two frames are not compatible with the known inclination of the sun's rays. If we tried to take into account a different optic (for example the 18mm Kern lens), things could only get worse. With an 18 mm focal length, the shadow would not be able to enter the field in either frame due to the narrower field of view.

If we consider the length of shadow according to the Hasselblad camera images and confirmed by the shadows of the stones of the scenario taken by the Maurer DAC, therefore taking into account an inclination of the sun's rays of 39°, the optical model we are verifying is more acceptable, although not yet effectively validated:

$$\text{Length(Shadow)} = \frac{2.00\ \text{m}}{\tan(39)} = 2.47\ \text{m}$$

In fact, it would remain out of frame for:

Frame 1, with 10 mm focal length: $Length\ of\ visible\ shadow = 2.47 - \frac{P_{min}}{\cos(25°)} =$ -0.69 m

Frame 2, with 10 mm focal length: $Length\ of\ visible\ shadow = 2.47 - \frac{P_{min}}{\cos(25°)} =$ -0.28 m

From Figure E13 we can also check the distance between the subject and the origin of the operator's shadow (fairly convergent with that expressed in E.1.3):

Subject – P_{min} = 4.99 m

Relevant component of the Shadow on the measurement plane = 2.47 m * cos(25°) = 2.24 m

P_{min} – Operator = 2.24 m – 0.35 m = 1.89 m

Distance between subject and operator = 6.88 m

Distance Subject – Lens = $\sqrt{6.88^2 + 1.6^2} = 7.06$ m

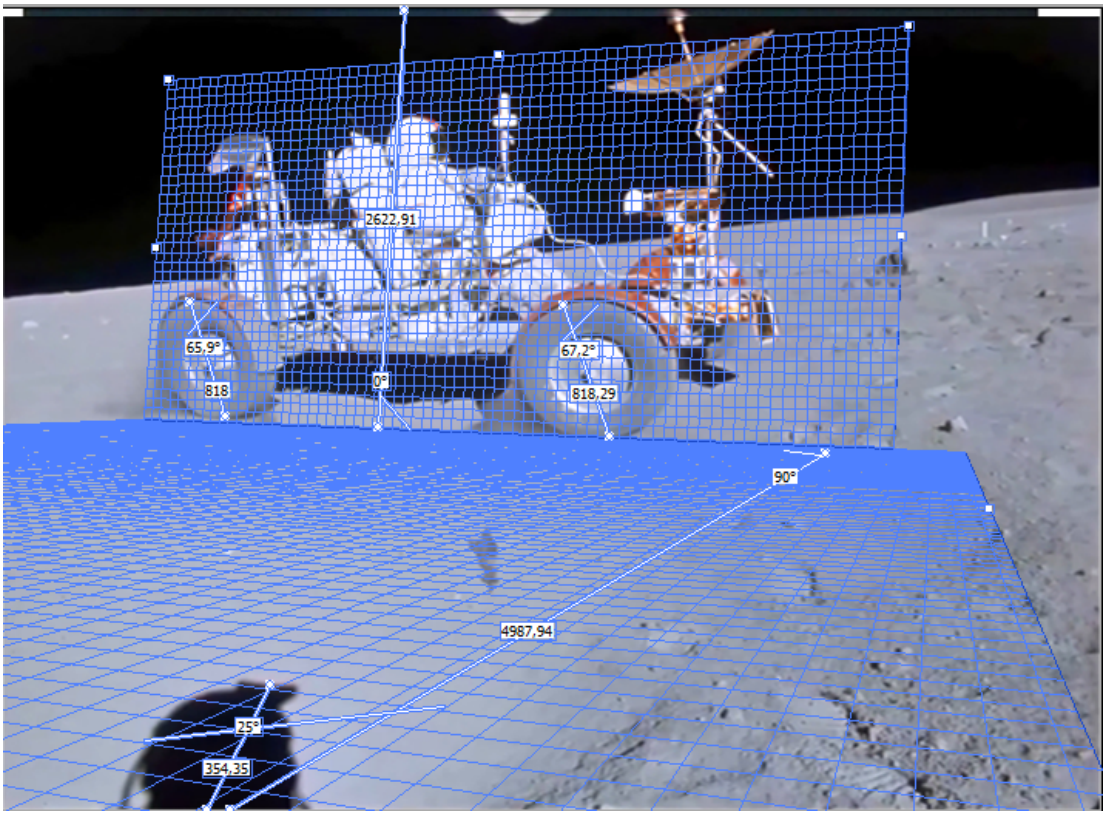

Figure E13 - Lunar Rover Grand Prix, EVA 1, measurement of Pmax on frame 2

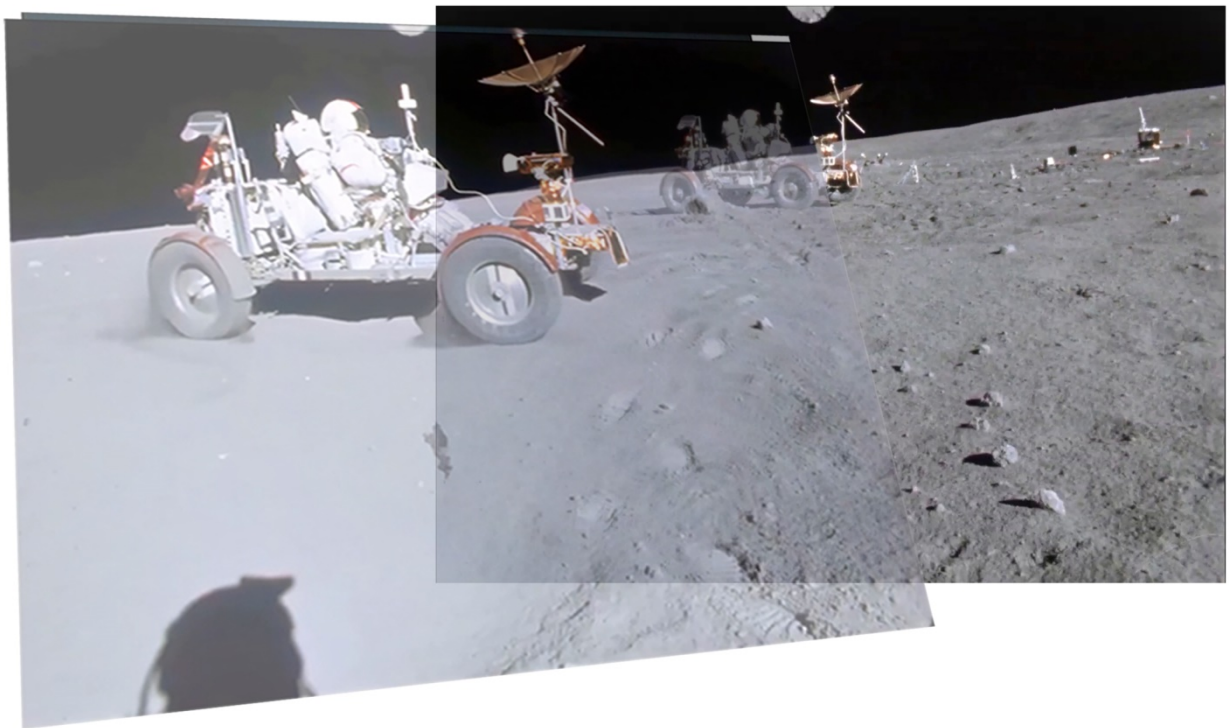

Figure E14 - LR Grand Prix, superposition of the analyzed frames taking into account the camera oscillations

By superimposing the two frames examined (Figure E14) we understand that in Frame 1 the shadow is projected off-screen because it is lateral to the frame. During the sequence, it comes into

the frame at various moments, due to the continuous oscillations of the camera, and in Frame 2 it reaches its maximum visibility. Its component relative to the optical axis would still be positive even in Frame 1 if the direction in which the lens is pointed allowed it to be framed because it reaches the vertex of the last boot print visible on the lunar soil, present for a handful of centimeters even in the initial frame.

The length of the visible shadow remains an element of discordance between the identified optical model and experimental data. This measurement depends on the inclination of the sun's rays, on $P_{min,}$ and minimally by the angle with which the shadow itself departs from the optical axis.

If in E.1.5 we sufficiently supported the data used as inclination of sunlight, in E.1.6 we were not able to return reliable data on the height above the ground of the Maurer DAC in the hands of Charles Duke, but only a hypothesis formulated on the basis of usual practices of the Apollo missions. Let's therefore check the height values of the H_{DAC} cine camera with the help of a spreadsheet [*Ann E4*].

With H_{DAC} = 1 m we easily discover that the main values of the proposed geometric model are very close to the measured ones (please compare Figure E9 for Frame 1 and Figure E13 for Frame 2):

Focal Length	**10**	mm
Field Angle	41.06	°
(H_{DAC}) Height of the Maurer Camera above the ground	1.000	mm
Angle of the sun's rays	39	°
Operator height	2.000	mm
Length of the operator's Shadow	2.470	mm
Shadow optical axis angle	25	°
Frame 1 ("Start")		
LRV wheel diameter	**818**	mm
Wheel diameter on the photo sensor	0.6	mm
Distance LRV-DAC according to the wheel aspect ratio	**13.633**	mm
(Dx) Ground line component of the distance	13.597	mm
(Dx') Distance on the ground line from image center and LRV	3.059	mm
Camera tilt angle	5.42	°
Camera tilt angle with respect to the operator	64.05	°
(**P_{min}**) Closest point framed on the ground	2.055	mm
(**P_{max}**) Highest point that can be framed above the LRV	4.671	mm
Length of the visible shadow	**203**	mm

Frame 2 ("Shadow")		
LRV wheel diameter	818	mm
Wheel diameter on the photo sensor	1,2	mm
Distance LRV-DAC according to the wheel aspect ratio	**6.817**	mm
(Dx) Ground line component of the distance	6.743	mm
(Dx') Distance on the ground line from image center and LRV	829	mm
Camera tilt angle	7.01	°
Camera tilt angle respect to the operator	62.46	°
(**P_{min}**) Closest point framed on the ground	1.918	mm
(**P_{max}**) Highest point that can be framed above the LRV	2.622	mm
Length of the visible shadow	**354**	mm
Difference between points Pmin (s)	137	mm

Table E1 – Reconstruction of the geometric model of the Maurer DAC images and optical system used

If our measurements are correct, they seem to place the camera's objective height at about 1 meter above the lunar surface, a hypothesis that suggests the camera was not attached to the ring prepared on the space suit, but which does not contradict what was stated by the *Lunar Surface Journal* (see E.1.6).

In conclusion, pending further review, our measurements seem to confirm that the focal length declared by NASA in the mission registers (10 mm). The distance of the lens from the LR in frame 1 seems to be 13.63 m and in frame 2 seems to be 6.82 m. Astronaut Charles Duke's statement reported on the *Lunar Surface Journal*, according to which the shooting was taking place about 50 meters away from the LR, seems not to be supported by our measurements even if we assume the use of the 18 mm Kern lens. [10]

E.2.1 Analysis of the motion of the Rooster Tails with Photoshop CS6

The motion of the dust kicked up by the LRV as Rooster Tails is tracked in the CLIP1 frames, the first sequence analyzed by Mihály Horányi and Hsiang-Wen Hsu in "**Ballistic motion of dust particles in the Lunar Roving Vehicle dust trails**" (see the Introduction to this study), using however, instead of the video converted to the 29 fps television standard, the most recent HD video versions of the Maurer DAC footage, released by NASA in 2019 [1]. These are 41 frames in total plus a "0" frame (prior to the sequence) on which the measurement system is calibrated. The last 7 frames do not seem to be able to give reliable results on the position of the rooster's head tail, therefore they are not present in the PSD file, and no measurements are carried out on them.

[10] *If any errors in our calculations or methodology are identified, we would be grateful for feedback. Alternatively, if the calculations are correct, it is possible that inaccuracies in the recorded mission data or materials specifications, could explain the discrepancies.*

We use the Vanishing Point Filter of Adobe Photoshop CS6 to resolve the spatial model of the environment in which the sequence takes place, in order to correctly identify a measurement plane and a coordinate system that allows us to trace the motion of the dust raised by LR [*Ann. E5*].

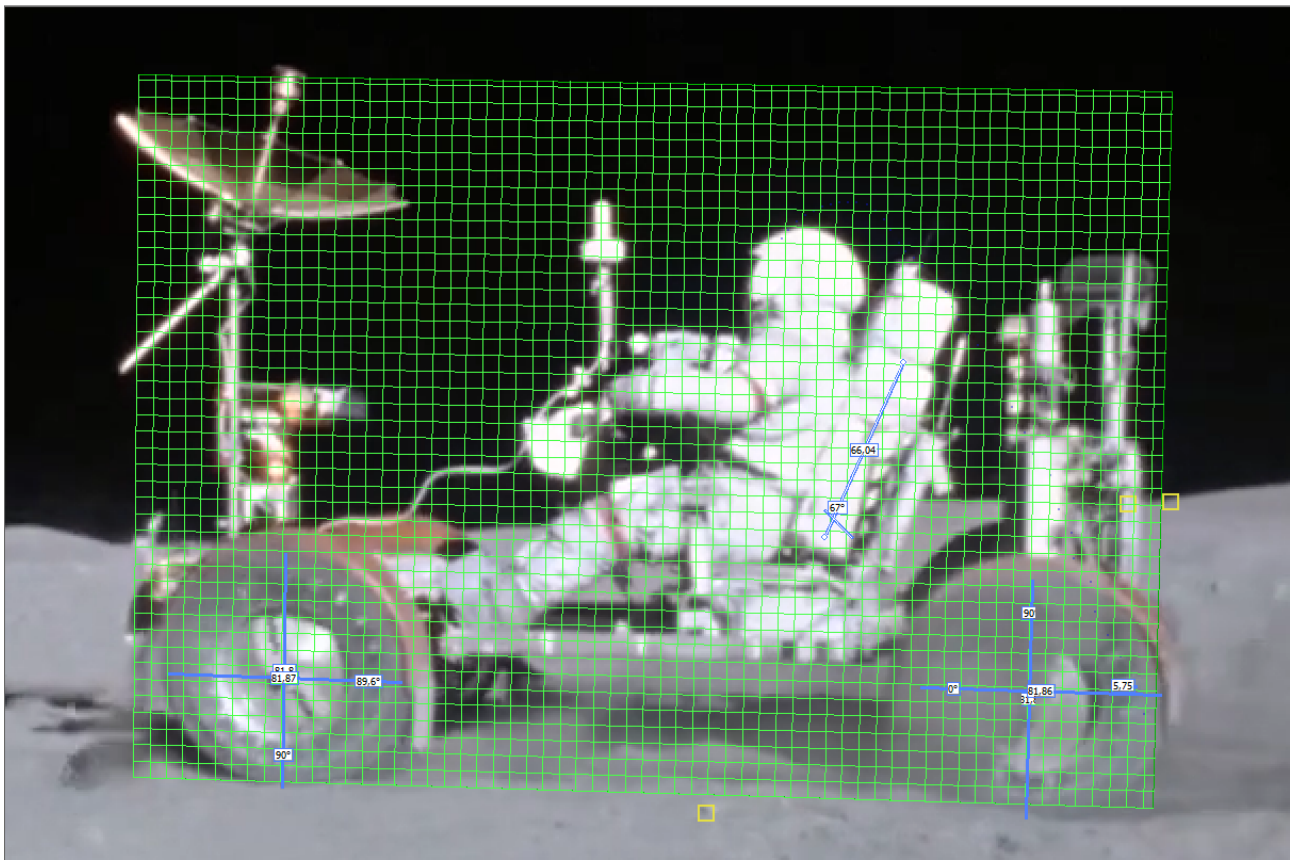

Figure E15 - Lunar Rover Grand Prix, EVA 1, CLIP 1 frame n° 0. Calibration of the measurement system.

While taking into account the considerations made in the previous paragraphs, with the intention of defining a measurement scale comparable to that used in the study "**Ballistic motion of dust particles in the Lunar Roving Vehicle dust trails**" by Mihály Horányi and Hsiang-Wen Hsu, we are conventionally assumed as known dimensions:

- LR wheel diameter: 81.8 cm
- PLSS height: 66.04 cm

The maximum altitude reached by the rooster tail is measured in each frame with respect to the closest point on the ground taken as a reference for stabilizing the sequence, as well as the horizontal component of the point of maximum elevation with respect to the position of the reference point on the ground. [*Ann. E6*] The results are reported in Table E4. Their analysis in order to identify the best fit is carried out with Origin Pro 2018.

We note that on the X-axis, the motion of the dust and that of the Rover have the same direction. This can be explained by assuming that the dust trail, overcoming the obstacle of the fender, was launched outwards starting from the upper portion of the Rover's wheel, since - as shown in image

E16 - if it had come out from the lower portion of the wheel, would have an opposite direction to that of the vehicle.

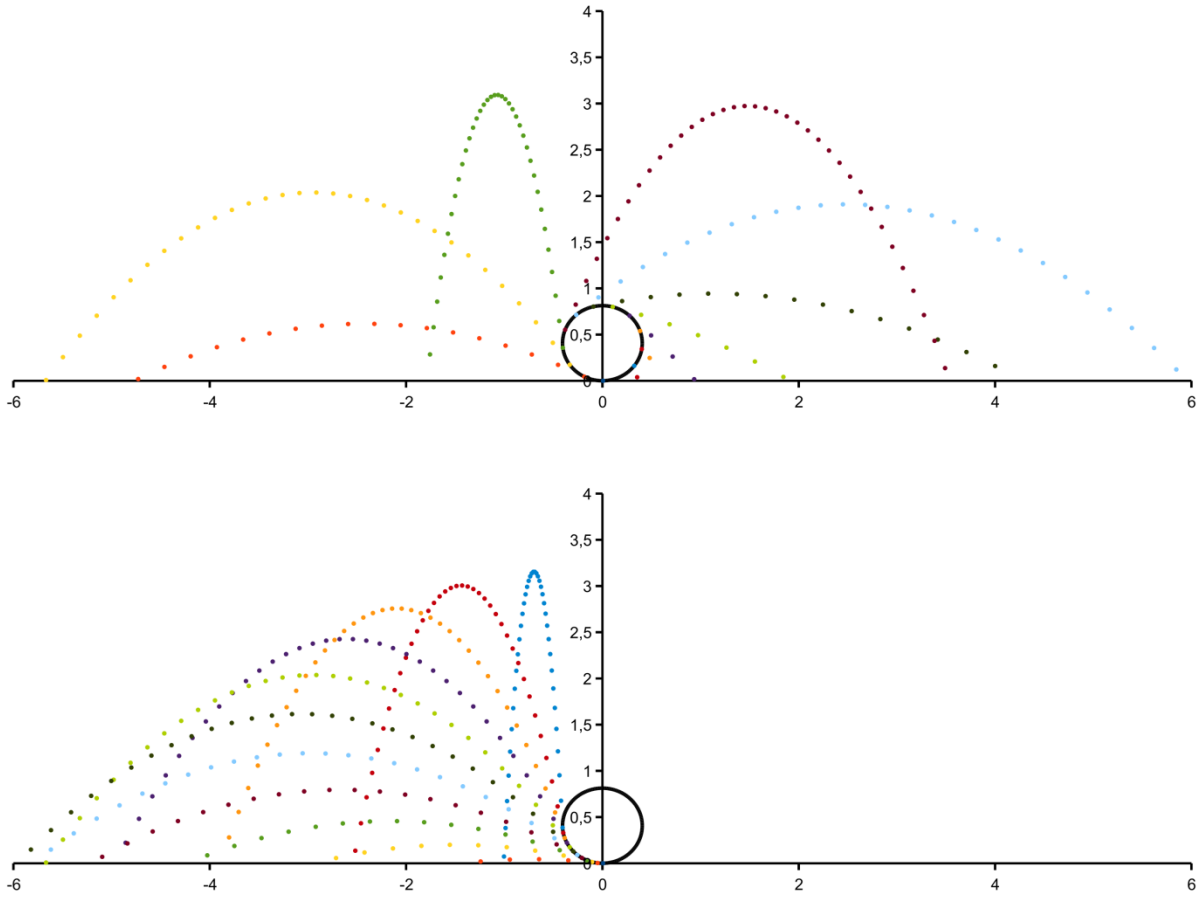

Figure E16 – Direction of the motion of the dust trail as a function of the point of separation from the wheel

For the Z axis, a second-degree polynomial fit is obviously proposed [*Ann. E7*]:

E1) $Z(t) = Y = Intercept + B1 * t + B2 * t^2$

As can be seen from Figures E17 and E18, the best estimation of the gravitational acceleration acting on the sequence under investigation is $\frac{1}{2}\ g_{or} = -1.40 \pm 0.04$ m/s ^{2} from which $g_{or} = -2.80 \pm 0.08$ m/s^2. A value once again inconsistent with that expected:

$$\frac{|g_{or} - g_m|}{\sigma} = \frac{|-2.80 + 1.62|}{0.08} = 14.75 > 3$$

The analysis of data variability proposed by the Origin Pro 2018 software shown in Figure E19 highlights disordered residual distribution (6 sign changes), normally distributed random error, and variance, confirming the quality of the tracking.

As regards the X axis, a linear model is proposed as a first test [*Ann. E12*]:

E2) $y = a + b * x$

As can be seen from Figure E20, the data collected from the tracking fits almost perfectly the linear model. The variance analysis returned by the Origin Pro software highlights a somewhat problematic result (Figure E21) which however does not affect the credibility of the hypothesis.

If the measurements taken will be confirmed by reviews and by a possible future audit [10], this would lead to the conclusion that the sequence did not retain its original speed, that the objects captured have different sizes, or that it was not shot in the environment in which the Apollo XVI mission actually took place.

If any errors in our calculations or methodology are identified, we would be grateful for feedback.

Frames	T(s)	Z (m)	X (m)
0	0.000	0.3(55)	1.5(03)
1	0.042	0.4(42)	1.4(65)
2	0,083	0,5(29)	1,4(27)
3	0,125	0,6(19)	1,3(88)
4	0,167	0,7(29)	1,3(50)
5	0,208	0,8(38)	1,3(10)
6	0,250	0,9(25)	1,2(71)
7	0,292	1,0(18)	1,2(33)
8	0,333	1,0(93)	1,1(94)
9	0,375	1,1(94)	1,1(56)
10	0,417	1,2(85)	1,1(17)
11	0,458	1,3(58)	1,0(72)
12	0,500	1,4(28)	1,0(33)
13	0,542	1,5(00)	0,9(96)
14	0,583	1,5(73)	0,9(58)
15	0,625	1,6(37)	0,9(19)
16	0,667	1,6(87)	0,8(83)
17	0,708	1,7(30)	0,8(47)
18	0,750	1,7(66)	0,8(09)
19	0,792	1,8(07)	0,7(72)
20	0,833	1,8(44)	0,7(35)
21	0,875	1,8(66)	0,6(97)
22	0,917	1,9(01)	0,6(60)
23	0,958	1,9(29)	0,6(22)
24	1,000	1,9(51)	0,5(88)
25	1,042	1,9(59)	0,5(48)
26	1,083	1,9(66)	0,5(12)
27	1,125	1,9(71)	0,4(75)
28	1,167	1,9(77)	0,4(39)
29	1,208	1,9(55)	0,4(03)
30	1,250	1,9(24)	0,3(67)
31	1,292	1,8(96)	0,3(23)
32	1,333	1,8(36)	0,2(90)
33	1,375	1.7(63)	0,2(39)
34	1,417	1.6(74)	0,1(96)

Table E2 – CLIP1, motion of the Rooster Tail maximum elevation point

Operation Time	07/12/2023 02:55:19
Equation	y = Intercept + B1*x^1 + B2*x^2
Report Status	New Analysis Report
Weight	Instrumental
Special Input Handling	
Data Filter	No

Input Data

Masked Data - Values Excluded from Computations

Bad Data (missing values) -- Values that are invalid and thus not used in computations

Parameters

		Value	Standard Error	t-Value	Prob>|t|
B	Intercept	0,27551	0,01736	15,86692	0
	B1	3,05356	0,05672	53,83577	0
	B2	-1,4052	0,0387	-36,31175	0

Standard Error was scaled with square root of reduced Chi-Sqr.

Statistics

	B
Number of Points	35
Degrees of Freedom	32
Residual Sum of Squares	104,93537
R-Square (COD)	0,99522
Adj. R-Square	0,99492

Summary

	Intercept		B1		B2		Statistics
	Value	Standard Error	Value	Standard Error	Value	Standard Error	Adj. R-Square
B	0,27551	0,01736	3,05356	0,05672	-1,4052	0,0387	0,99492

ANOVA

		DF	Sum of Squares	Mean Square	F Value	Prob>F
B	Model	2	21827,73606	10913,86803	3328,17988	0
	Error	32	104,93537	3,27923		
	Total	34	21932,67143			

At the 0.05 level, the fitting function is significantly better than the function y=constant.

Figure E17 – Origin Pro fit result of the Z-axis motion curve: parameters obtained and their reliability

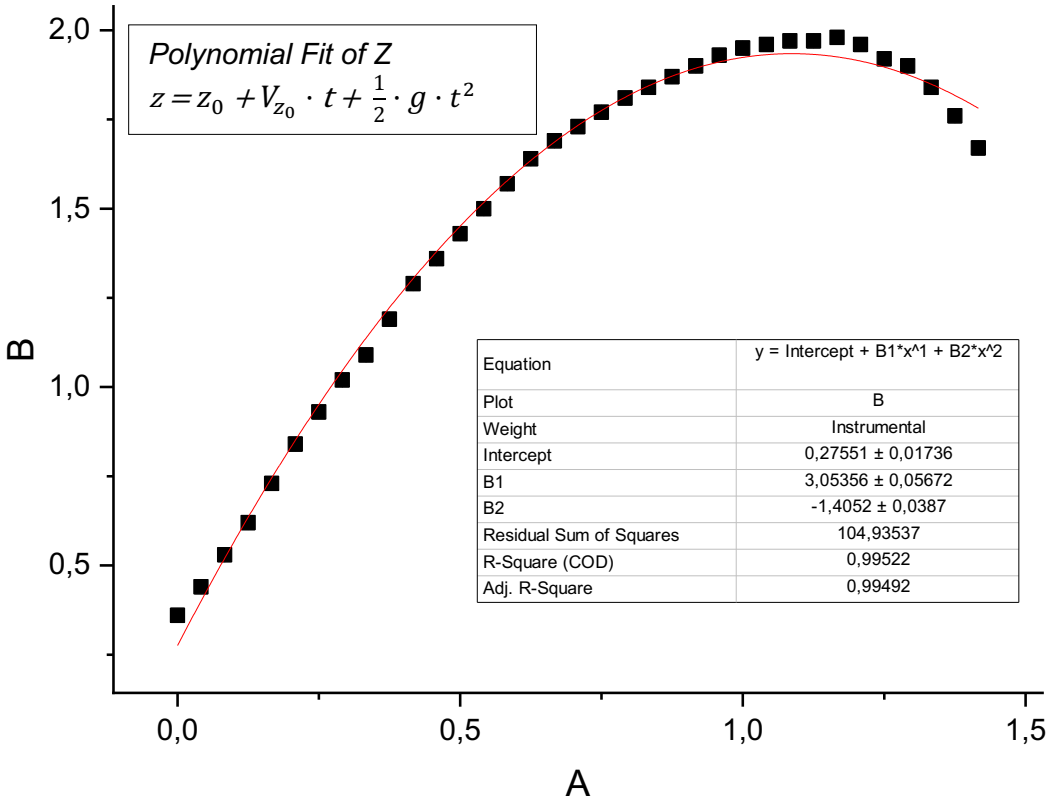

Figure E18 – Origin Pro 2018: comparison graph between the theoretical model (red) and data detected on the Z-axis

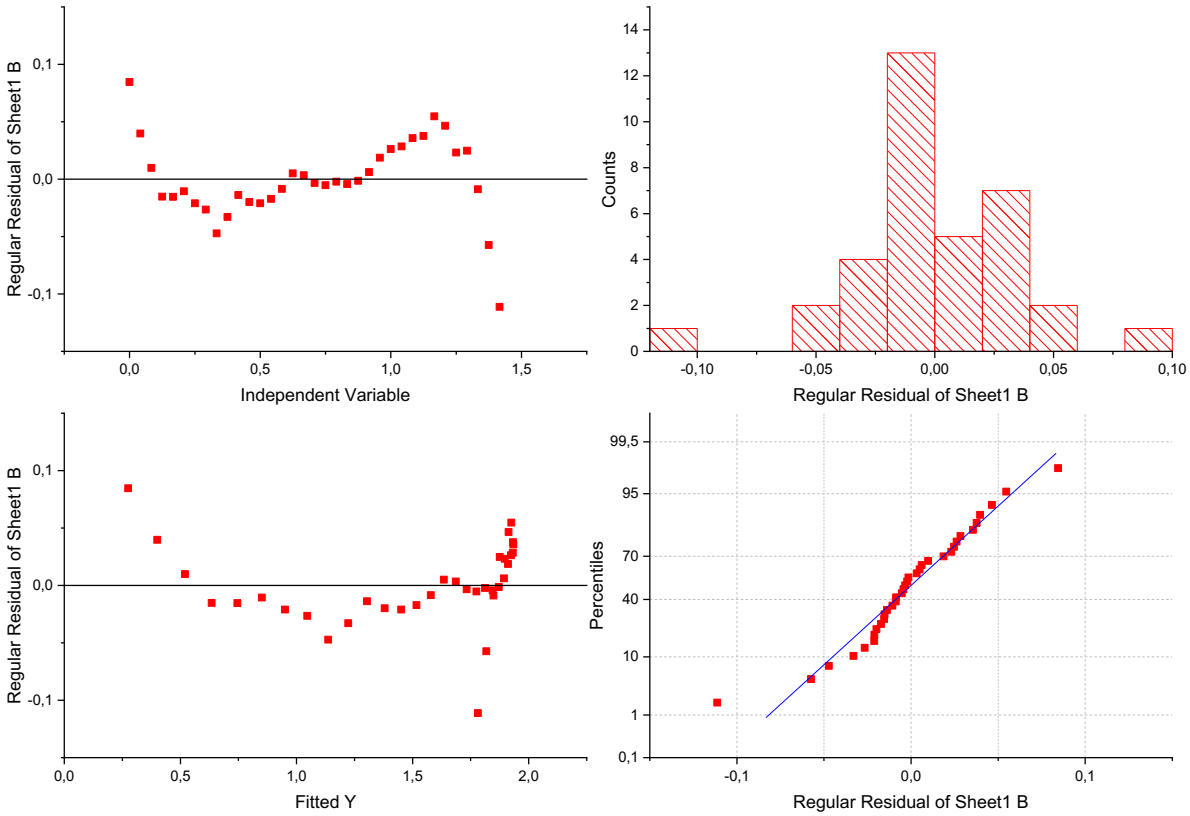

Figure E19 – Origin Pro 2018: data variability with respect to the equation of motion identified on the Z-axis

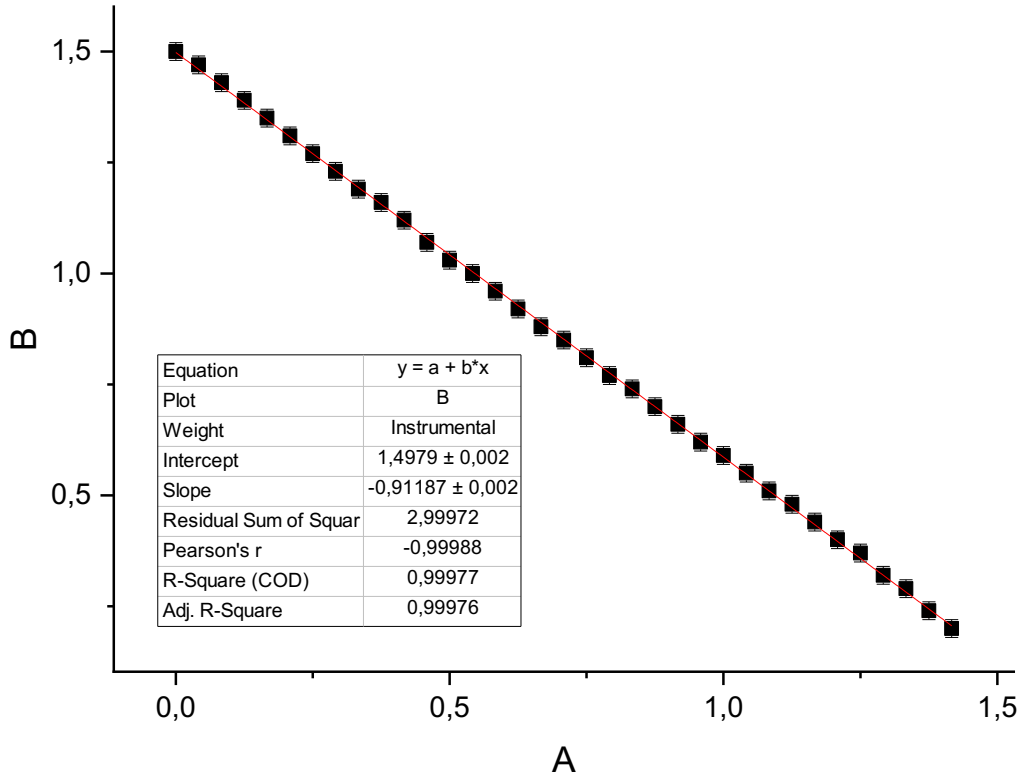

Figure E20 - Origin Pro 2018: comparison graph between linear theoretical model (red) and data detected on the X-axis

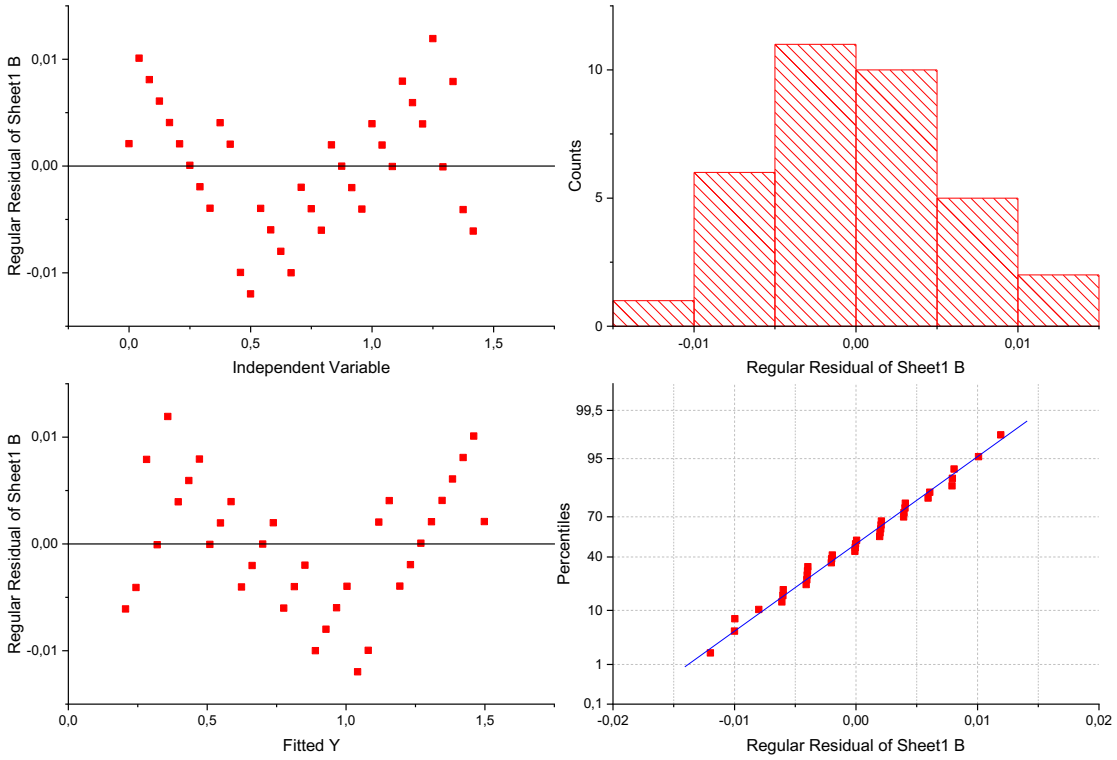

Figure E21 - Origin Pro 2018: data variability with respect to the equation of motion identified on the X-axis

A comparison is made with a second model, in which the air resistance is hypothesized according to the equation already used in C.4.4.2 (Plot in Figure E23):

E3) $X_{modT}(t) = O + V * h * (1 - e^{t/h})$

Considering the physical characteristics of the lunar regolith simulant LSS-4 and the alteration of the shooting frame rate demonstrated by the fit on the Z axis, the parameter h identified in C.4.1, in this context applies:

$$0.62 * \sqrt{\frac{9.81}{2.20}} = 1.16 \text{ s}$$

As can be seen from Figure E23, although this model exceeds the 95% confidence threshold, it is much less reliable than the previous one. Thanks to Origin Pro we carry out three comparison tests of the E2 and E3 models: Akaike (AIC) / Bayesian Information Criterion (BIC), F-Test. Although there is not enough information to draw conclusions from the F-test, the other two tests clearly reveal the greater reliability of the linear model (Figure E22).

Fit Comparison of Models

Notes

Description

	Model1	Model2
Input Data	[Book1]Sheet1!(A,B,C)	[Book1]Sheet1!(A,B,C)
Fit Report	[Book1]FitLinear1	[Book1]FitNL1
Equation	y = a + b*x	X = o + v*h*(1 - exp(-t/h))
Function		HorizontalAirDrag (User)
Number of Points	35	35
Number of Parameters	2	2

Preferred Model

	Model Name
AIC	Model1
BIC	Model1
F-Test	No conclusion

Akaike's Information Criterion Test (AIC)

	RSS	N	Params	AIC	Akaike Weight
Model1	2,99972	35	2	-79,21483	1
Model2	356,80036	35	2	88,03819	4,80253E-37

Model1 has lower AIC value and so is more likely to be correct.
This model is 2.08224e+036 times more likely to be correct.

Bayesian Information Criterion Test (BIC)

	RSS	N	Params	BIC	Diff BIC
Model1	2,99972	35	2	-75,32298	0
Model2	356,80036	35	2	91,93004	167,25301

Model1 has lower BIC value and so is more likely to be correct.
BIC difference greater than 10 gives decisive conclusion that Model1 is correct.

F-test

	F	Numer.DF	Denom.DF	Prob > F
	--	0	33	--

There is not enough information to draw conclusion

Fit Parameters

Fit Statistics

Figure E22 – Origin pro; Rooster Tail, Clip1, comparison between the models E1 and E3

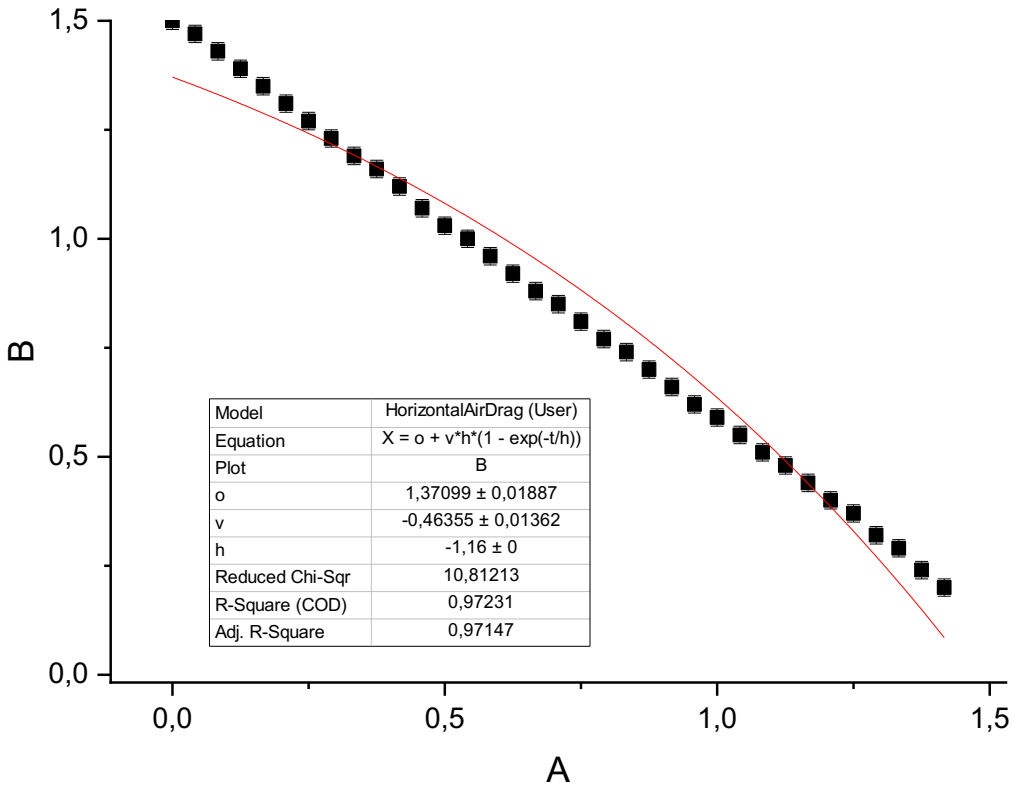

Figure E23 - Origin Pro 2018, Clip1, comparison: model with air resistance (red) and data collected on the X-axis

E.3.1 Rover jump and vehicle dimensions

During the return phase of the first lap of the Lunar Rover Grand Prix, the vehicle undergoes significant dynamic stress caused by the roughness of the ground. About one minute from the sequence start it finds along its path a crater whose surface length is slightly lower than the Rover wheelbase and whose depth is a few centimeters less than the radius of the wheel (about 36 cm). Upon exiting the depression, the Rover takes its wheels off the ground for about 1 second with the only interference due to the impact of the rear wheel on the ascending wall of the depression, an impact which was largely absorbed by the shock absorber - suspension system. This circumstance is interesting for determining some fundamental elements of the sequence.

We know from various sources that the LRV's performance allowed a speed between 0 and 14 km/h (3.89 m/s). [11] Each wheel was equipped with an autonomous electric motor. The suspensions were torsion bars. From the video already indicated in E.1.1, taking a fixed reference on the ground, we can observe that the vehicle, just before the leap we are dealing with in this paragraph, was able to cover the distance equivalent to its wheelbase (2.286 m) [10] in approximately 21/24 second (V_x = 2.61 m/s).

The crater slows down the vehicle slightly, given that the same measurement carried out on the LRV at the exit from the depression highlights coverage of the same distance in 23 frames (2.38 m/s). The clip slowed down to 1 fps is available at this address:

https://www.youtube.com/watch?v=WKswkQAcayA

---

[11] *https://www.nasa.gov/wp-content/uploads/static/history/alsj/LRV_OpsNAS8-25145.pdf Lunar Roving Vehicle Operation Handbook, page 184, page 13, The Boeing Company LRV Systems Engineering, Huntsville (Alabama, USA) April 19, 1971* [*Ann. 6*]

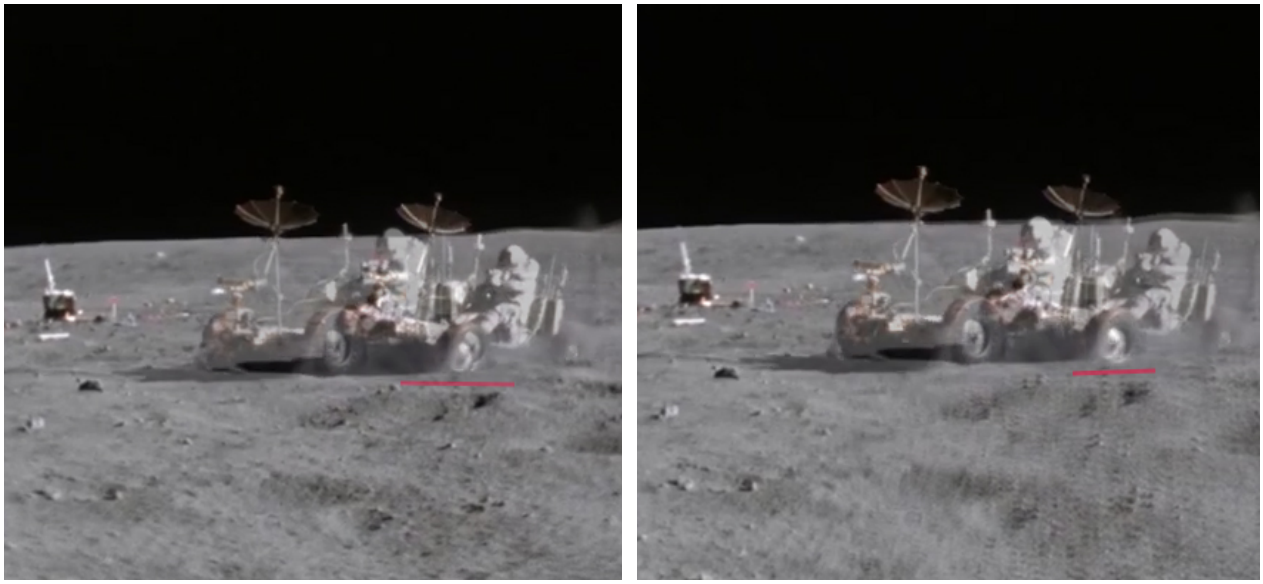

Figure E24 - Overlap of Frames 1 - 22 and 1 - 23 of the sequence with YouTube code WKswkQAcayA

The superposition of two frames between which 23/24 seconds pass confirms the speed just declared at the exit from the crater. The rear wheel captured in the second image coincides with the front one in the first frame extracted here. The Rover exceeded the speed threshold of 8.5 km/h, foreseen by the technical manuals as the limit for the stability of the vehicle in the presence of uneven ground (rough Mare) [12].

We will track the motion of the chassis, of the Rover front end, and of the front wheels center, starting from the entry of the latters into the crater and for the entire duration of the jump, until the subsequent landing, following the usual procedures in order to extract frames from the best quality video available, correcting format and geometric aberrations [*Ann. E9*] [*Ann. E10*]. The instrumental error in measuring the sequence is 1 px = ± 0.01 m and the accuracy error is equally large.

As regards the identification of the Center of Mass, we use the coordinates provided by NASA [10] whose projection on the external axis of the chassis corresponds to the point indicated in Figure E25 as the center of the "Outboard Handhold" which offered comfort and stability to the astronauts while the running.

It should be noted that the available Center of Mass coordinates refer to the vehicle in fully loaded conditions. In the sequence, it is clearly visible how the presence of only one astronaut on board makes the vehicle more subject to lateral inclinations (roll). About 45% of the Rover's total mass when it was fully loaded was the mass of the two astronauts. It is not possible to correctly locate the Center of Mass and trace it from the available images.

---

[12] *https://www.lpi.usra.edu/lunar/documents/NTRS/collection2/NASA_TM_X_66816.pdf LRV Operation Handbook Appedix A (Perfomance Data), page A-44, The Boeing Company Huntsville (Alabama, USA) April 19, 1971* [*Ann. E11*]

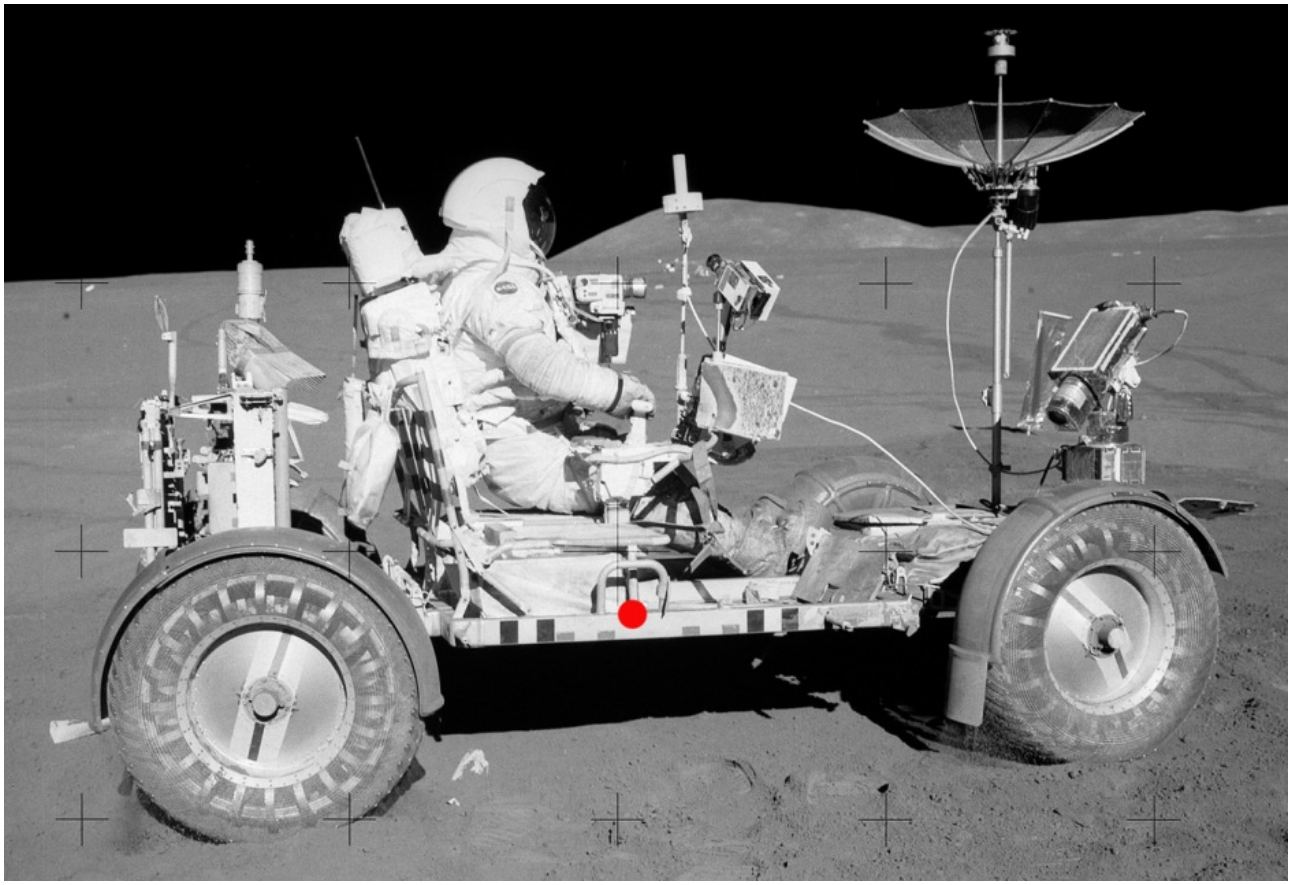

Figure E25 – LRV Center of Mass External projection, Apollo 15 - AS15-85-11471HR – David R. Scott driving [13]

The image quality is much better than those shot with CTV. These are not recombined video frames, but images printed on film, therefore the method of determining the accuracy error used in the previous sections does not apply. Nonetheless, an accuracy error can be defined for each tracked object based on the respective crowns of pixels that identify their contour and that's worth at least another pixel.

From the images, it is not possible to determine the exact internal conformation of the depression. The lunar soil was characterized by good bearing capacity and poor stability of the slopes, however, given the modest dimensions of the crater, of course for the model we can use the simplified geometry represented in Figure E26.

It is possible to obtain the angle of inclination of the dip walls starting from the measurements taken, in particular from tracking the motion of the central pin of the Rover front left wheel when it enters and exits the dip.

---

[13] http://www.hq.nasa.gov/wp-content/uploads/static/history/alsj/a15/AS15-85-11471HR.jpg *Apollo 15 Map and Image Library Copyright © 1996-2016 by Eric M. Jones. All rights reserved. HTML Design by Brian W. Lawrence. Last revised 23 November 2016.*

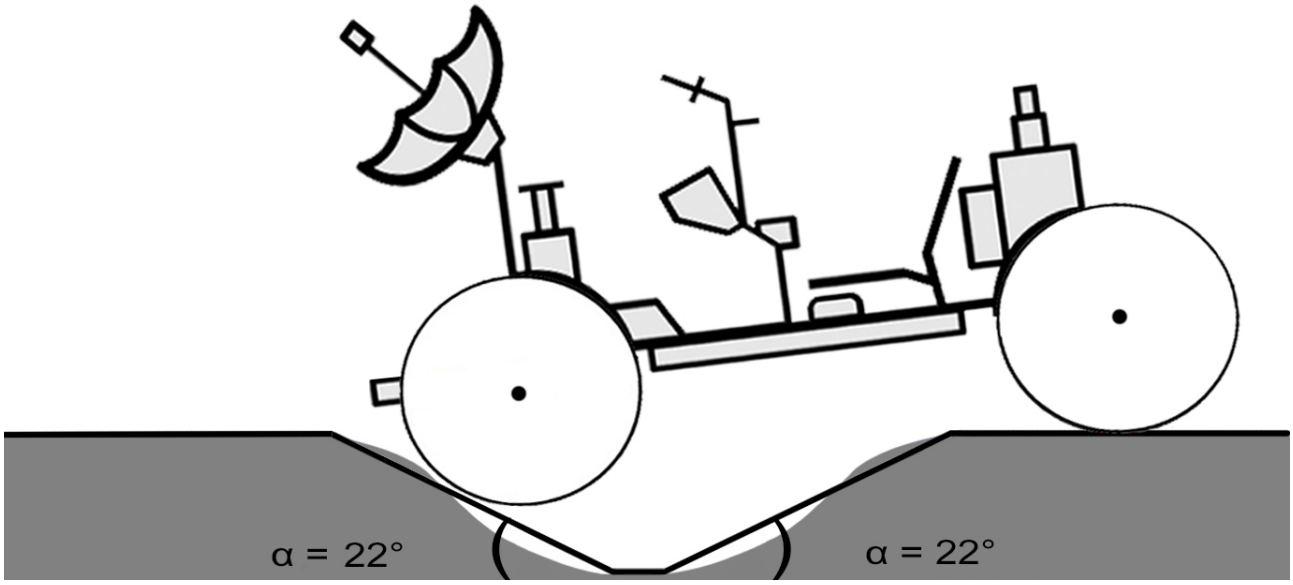

Figure E26 – Geometric approximation of the crater crossed by the LRV during the first phase of the Grand Prix

The wheel takes 18 frames to cross the dip, 9 frames for the descending part and the same number for the ascending part, the two walls are therefore arranged symmetrically and with a similar inclination.

$$\alpha = \text{Arctan}\left(\frac{crater\ depth}{\frac{9}{23} LRV\ \text{wheelbase}}\right) = \text{Arctan}\left(\frac{0{,}36\ m}{\frac{9}{23} * 2{,}286\ m}\right) = 22°$$

The role of the suspension-shock absorber system is obviously to isolate the chassis from the stresses exerted by the ground and to guarantee the best possible adhesion of the wheels to the driving surface at all times. Part of the energy from impacts suffered by the vehicle's wheels is dissipated by this system but it is inevitable that a variable quantity of this energy is still transferred to the chassis. The vehicle therefore suffers pitching thrusts, caused by the stresses exerted by the ground which the suspensions are unable to absorb completely.

These thrusts, moreover, were already evident before the vehicle entered the crater. In the frames immediately preceding the ones being measured, we can already note a significant longitudinal oscillation of the front end caused by the presence of potholes and bumps that the Rover overcomes on its path.

In the sequence under analysis, due to the crater crossing and the previous thrusts, the front end is subjected to a vertical inertia which causes it to lift, with consequent load transfer towards the rear axle and rotation around the Center of Mass. The behavior of the vehicle just described is compatible with the available technical information, also considering the position of the Center of Mass, set back by approximately 30 cm compared to the midpoint of the longitudinal axis. The technical manual - as already mentioned - advised the pilots not to proceed with a speed like the one filmed in this part of the sequence, over the stability threshold of the vehicle.

With the entry of the rear wheels into the crater, two frames after the complete ascent of the front wheels, the normal force exerted by the ground on the rear axle is worn out, a condition that determines the free fall of the rear part of the vehicle. The entire vehicle, which can be simplified in a single rigid body, is simultaneously in free fall and rotating due to the pitch thrust.

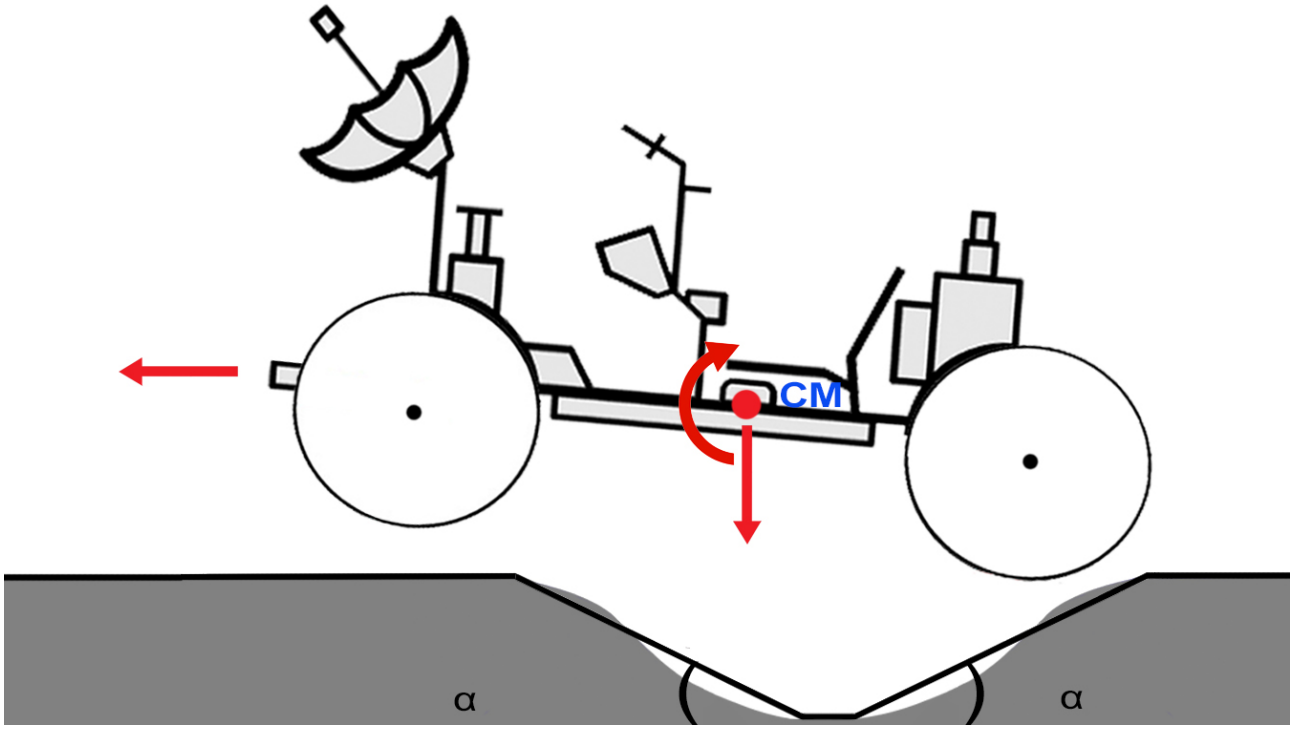

Figure E27 – Grand Prix sequence, Free fall of the LRV analysis of the rigid body motion components.

The rear wheels fall with an initial vertical speed equal to zero and as can be seen in the graph in Figure E28 they do not touch the descending wall of the crater. Continuing their fall, they successively lean on the ascending wall, meeting it between the frame T_{13} and the following T_{14}.

Up to the point P indicated on the graph in Figure E28 the wheels do not encounter resistance from the ground and do not lift significant quantities of regolith into the environment (as can be seen in the images). In T_{14} the rear wheels hit the ascending crater wall, and the impact generates an impulse sufficient to reverse the rotary motion but largely absorbed by the shock absorber-suspension system.

From T_{14} to T_{18} the rear wheels have to climb a further 0.20 m height difference, producing a limited torque thanks to the progressive compression of the suspension. After the rear wheel has overcome the obstacle and the torque is exhausted, the rotational motion stabilizes, returning to a constant angular velocity regime. The vehicle is again in free fall.

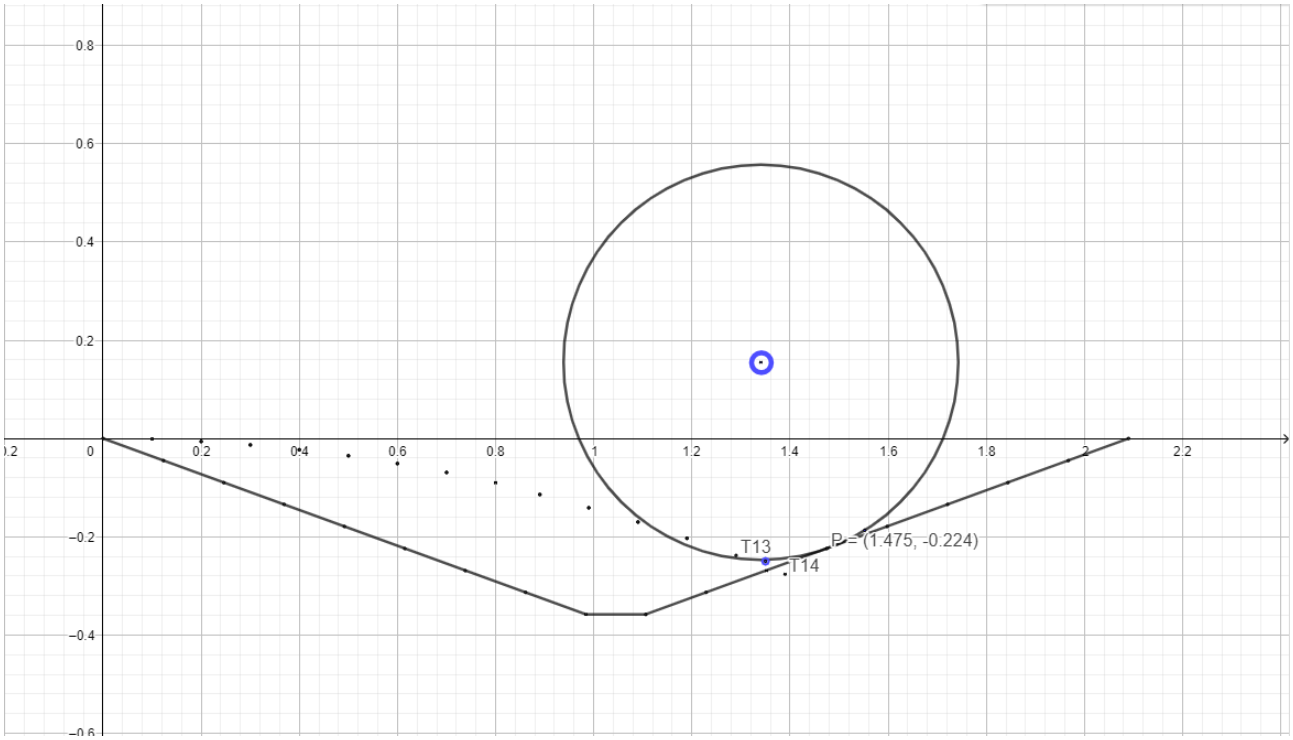

Figure E28 – Free fall of the LRV, contact between the rear wheel and the ground

The dynamics of the phenomenon just described highlights how from frame T_0 to frame T_{23} the motion of the front end can be approximated to a free fall motion combined with a uniform rotary motion. Between frame T_{13} and frame T_{14}, the rear wheels hit the depression-rising wall, causing a reversal of the rotary motion.

From frame T_{14} to frame T_{18} the rotary motion resumes with a slight acceleration due to the persistence of a torque counteracted by the suspensions. From frame T_{19} until the end of the vehicle's free fall in T_{23}, the rotary motion again acquires a constant speed. Performing a fit with Origin Pro (fig E30) effectively highlights what has been proposed theoretically up to this point.

Frames	Time(s)	X Rear Wheel (m)	Z Rear Wheel (m)
0	0.000	0.00	0,00
1	0,042	0,10	-0,00
2	0,083	0,20	-0,01
3	0,125	0,30	-0,01
4	0,167	0,40	-0,02
5	0,208	0,50	-0,04
6	0,250	0,60	-0,05
7	0,292	0,70	-0,07
8	0,333	0,80	-0,09
9	0,375	0,89	-0,11
10	0,417	0,99	-0,14
11	0,458	1,09	-0,17
12	0,500	1,19	-0,20
13	0,542	1,29	-0,24
14	0,583	1,39	-0,20
15	0,625	1,49	-0,16
16	0,667	1,59	-0,12
17	0,708	1,69	-0,08
18	0,750	1,79	-0,04

Table E3 – Distance between the front wheel pin and the chassis during the free fall

The point tracked on the front end is actually the end of the LRCU Unit, resting on the chassis and attached to it by two support pins (fig E29). The unit was 56 cm long and 15 cm thick [14]. Compared to the LRV known measurements, the distance of the traced point from the Center of Mass will therefore have to be increased, both horizontally and vertically:

Horizontal distance Front End - Centre of Mass: 1,85 m [10]
Vertical distance LRCU Unit - Centre of Mass: 0,15 m
Distance End of LRCU Unit - Centre of Mass: $1{,}85 + \sqrt{0{,}56^2 + 0{,}15^2}\, m = 2{,}43\, m$

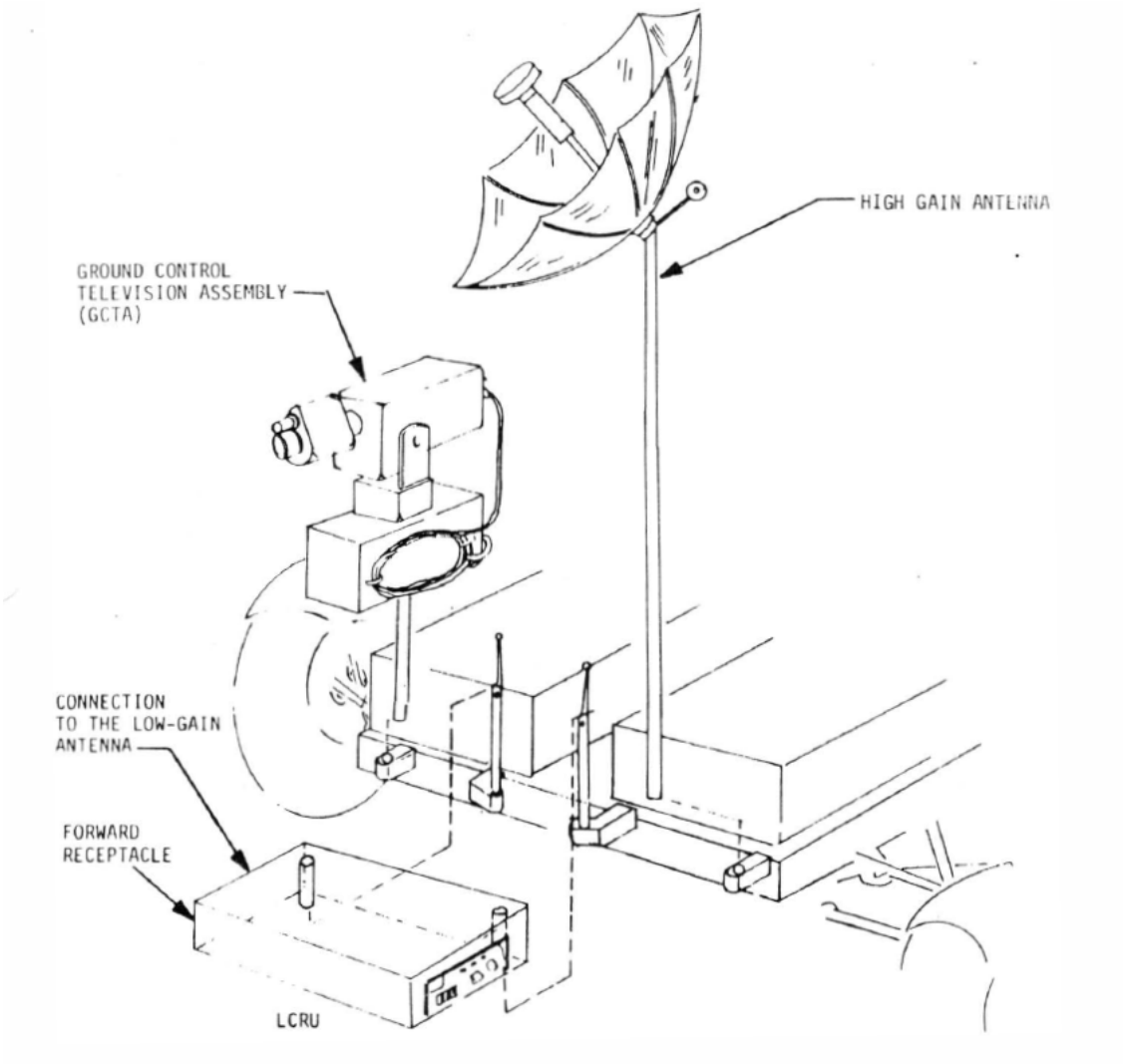

Figure E29 – Lunar Rover Handbook – LRCU Unit [15]

[14] *https://www.nasa.gov/wp-content/uploads/static/history/alsj/hsi-481184-lcru.pdf Crew Training Manual Lunar Communications Relay Unit, RCA Corporation, Camden, New Jersey, 3 0 March 1971*
[15] *https://www.lpi.usra.edu/lunar/documents/NTRS/collection2/NASA_TM_X_66816.pdf LRV Operation Handbook, page. 4-2, The Boeing Company Huntsville (Alabama, USA) April 19, 1971 [Ann. E11]*

Between T_0 and T_{13} the equation describing the motion of the frontend on the Z axis and integrating both the free fall of the rigid body and its rotational motion caused by pitching can be defined as follows:

$$E4) \quad Z(t) = Z_0 + v_0 t - \frac{1}{2} g t^2 + d \cdot sin(\theta_0 + \omega_0 t)$$

Dove:

- Z_0 is the initial vertical position of the point tracked at the end of the LCRU unit
- v_0 is the initial vertical velocity of the Center of Mass
- g it's the gravitational acceleration
- d it is the distance between the Center of Mass and the tracked point
- θ_0 is the initial tilt angle of the vehicle
- ω_0 is the initial angular velocity of the vehicle

The part that expresses the rotational motion of the equation

$$\boldsymbol{E5}) \quad \theta(t) = \theta_0 + \omega_0 t$$

can be studied separately. In the various frames of the sequence, we can detect the tilt angles of the LRV, and the data obtained can be fitted to verify which are the most effective values in validating the model for ω_0 and α. Given the low impact of the torque on the first part of the descending rotational motion and its short duration (5 frames) for the angles from frame T_{14} to frame T_{23} a linear fit will be attempted according to the simple variant of equation E5:

$$\boldsymbol{E6}) \quad \theta(t) = \theta_{t14} - \omega_0 t$$

Table E4 reports the data obtained from the measurements and, in the last column, the maximum error applicable to each measured angle. *[Ann. E10]*

To detect the tilt angles in the 24 frames of LRV free fall, the Photoshop CS6 Vanishing Focus Filter is used, positioning a measurement line in correspondence with the visible part of the chassis (in some frames the chassis is covered by the dust raised by the wheels). At the same time, the distance L_r between the two ends of the measurement line is noted, both in pixels and in mm: these are necessary data to calculate the maximum error applicable to the measurements of the identified angles, considering each pixel as one of the N elements of our measurement.

Let's consider two points (x_1, y_1) e (x_2, y_2) with a maximum error $\sigma_x = \sigma_y$ = 1 pixel (equivalent to 1 cm) for the experimental error + 1 pixel for the accuracy error = 2 pixel (2 cm). To calculate the overall error on the tilt angle, it is first necessary to consider the propagation of the error due to the measurement of the two points:

$$\sigma\theta = \left|\frac{d\theta}{d(x_2 - x_1)}\right| \sigma_x + \left|\frac{d\theta}{d(y_2 - y_1)}\right| \sigma_y$$

After deriving the expression for θ, we can approximate the error as:

$$\sigma\theta \approx \frac{1}{(x_2 - x_1)^2 + (y_2 - y_1)^2} * (|x_2 - x_1|\sigma_y + |y_2 - y_1|\sigma_x)$$

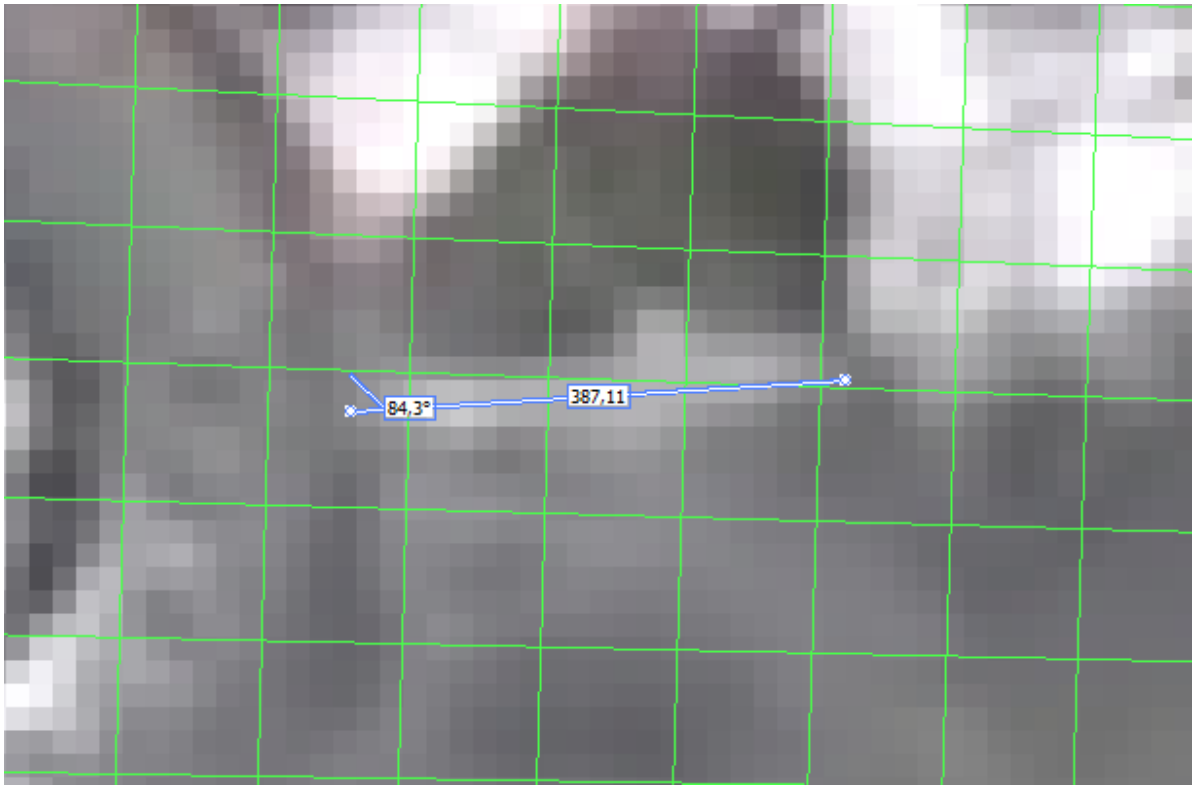

Figure E30 – Measurement of the LRV chassis tilt angle in the frame T_0

When we consider multiple points distributed along the side of the object, we can perform a linear fit to find the line that best fits those points. The line obtained through linear regression is of the type:

$$y = mx + q$$

where $m = tan(\theta)$ represents the slope of the line, and θ is the angle we want to detect. The regression minimizes the sum of the errors orthogonal to the line, and the error on m is proportional to the dispersion of the points around the line. The total uncertainty is distributed over more points, and the statistical variance of the estimate decreases with the number of samples N according to the law of large numbers.

$$\sigma_{\theta,fit} \propto \frac{\sigma_\theta}{\sqrt{N}}$$

Frames	Time (s)	θ °	rad	L_r (pixel)	L_r (m)	Max Err
0	0,000	-5,7	-0,0(99)	21	0,387	0,012
1	0,042	-4,5	-0,0(79)	22	0,384	0,012
2	0,083	-2,8	-0,0(49)	23	0,383	0,011
3	0,125	-1,6	-0,0(28)	22	0,385	0,011
4	0,167	-0,4	-0,0(07)	16	0,277	0,018
5	0,208	0,7	0,0(12)	16	0,274	0,018
6	0,250	1,9	0,0(33)	16	0,276	0,019
7	0,292	3,8	0,0(66)	25	0,420	0,010
8	0,333	5	0,0(87)	25	0,416	0,010
9	0,375	6,5	0,1(13)	26	0,431	0,010
10	0,417	7,9	0,1(38)	28	0,452	0,009
11	0,458	9,2	0,1(61)	23	0,382	0,012
12	0,500	10,5	0,1(83)	24	0,381	0,012
13	0,542	12,1	0,2(11)	19	0,301	0,018
14	0,583	13,3	0,2(32)	19	0,301	0,018
15	0,625	12,5	0,2(18)	18	0,284	0,019
16	0,667	11,5	0,2(01)	19	0,288	0,018
17	0,708	10,3	0,1(80)	19	0,280	0,019
18	0,750	8,9	0,1(55)	18	0,276	0,019
19	0,792	7,5	0,1(31)	18	0,266	0,020
20	0,833	6,1	0,1(06)	25	0,371	0,012
21	0,875	4,6	0,0(80)	25	0,369	0,012
22	0,917	3,2	0,0(56)	32	0,467	0,008
23	0,958	1,8	0,03(1)	33	0,465	0,008

Table E4 – LRV tilt angles and elements for calculating the maximum error

Using the Origin Pro software, the measurement data relating to the tilt angles are then fitted to detect the angular velocity (fig E31). The angles observed from T_0 to T_{13} are fitted first, and then we proceed with the angles of the frames from T_{14} to T_{23} (fig 32). [*Ann. E12*]

In figure 32 it can be observed that although the overall fit is effective with respect to a linear model, the rotary motion is slightly perturbed up to frame T_{18} by the acceleration caused by the torque. The rotation speed, although of opposite sign, is almost completely preserved in the descending phase with respect to the ascending phase.

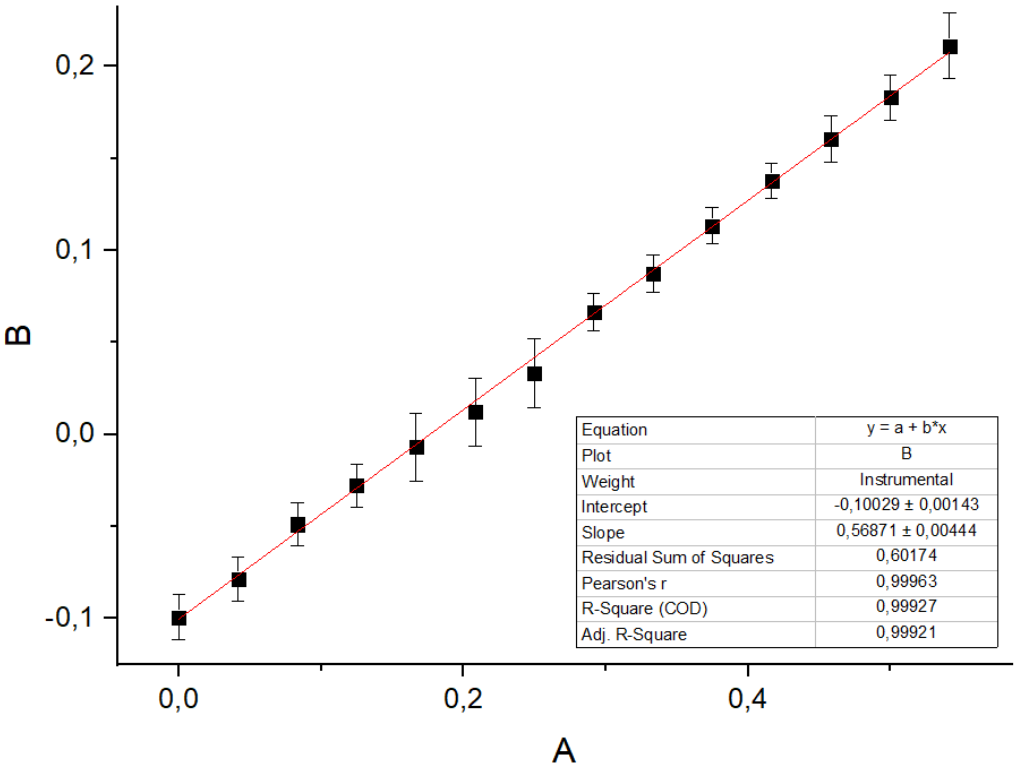

Figure E31 – Fit of LRV rotation due to the pitch between frames T_0 and T_{13} during the free fall

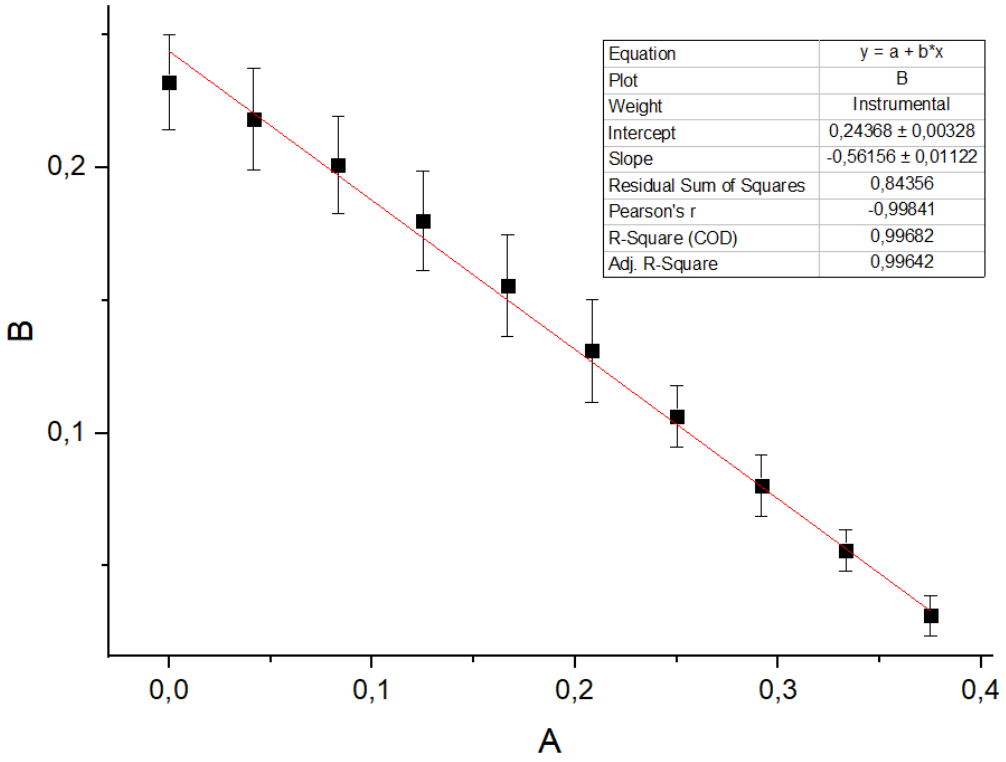

Figure E32 – Fit of LRV rotation due to the pitch between frames T_{14} and T_{23} during the free fall

We go to the Z-axis tracking of the LRCU Unit. The heights reached in the 24 frames of the free fall sequence are presented in Table E5 with the relative confidence intervals. For complete investigation data carried out please refer to the previous attachments [*Ann. E9*], [*Ann. E10*] which hosts the tracking on the vertical axis of a series of elements of the LRV, extended to the frames immediately preceding and following those in question.

Front	Time (s)	Event	Z_{LRCU} (m)	Max Error
0	0,000	Rear Wheels in the dip (Free Fall Phase Start)	0,5(2)	0,02
1	0,042	Rear Wheels in the dip	0,5(9)	0,02
2	0,083	…	0,6(3)	0,02
3	0,125	…	0,6(8)	0,02
4	0,167	…	0,7(4)	0,02
5	0,208	…	0,7(9)	0,02
6	0,250	…	0,8(3)	0,02
7	0,292	…	0,8(8)	0,02
8	0,333	…	0,9(4)	0,02
9	0,375	…	0,9(8)	0,02
10	0,417	…	1,0(1)	0,02
11	0,458	…	1,0(4)	0,02
12	0,500	…	1,0(4)	0,02
13	0,542	Rear Wheels Dip Touch	1,0(5)	0,02
14	0,583	…	1,0(5)	0,02
15	0,625	…	1,0(4)	0,02
16	0,667	…	1,0(4)	0,02
17	0,708	…	1,0(2)	0,02
18	0,750	…	1,0(0)	0,02
19	0,792	Front Wheels and Rear Wheels in free fall	0,9(8)	0,02
20	0,833	…	0,9(5)	0,02
21	0,875	…	0,9(1)	0,02
22	0,917	…	0,8(8)	0,02
23	0,958	Front Wheel landing	0,8(5)	0,02

Table E5 – Results of the LRCU Unit end tracking during the Lunar Rover free fall

The collected data are subjected to two different fits with the software Origin Pro 2018, the first one from T_0 to T_{13} and the second one from T_{14} to T_{23}. For both, equation E4 is proposed. Distance d between the end of the LRCU Unit and the Center of Mass is taken into account. = $2{,}43\ m$ as previously calculated and $\theta_0 = 0{,}0227 +/- 0{,}0085\ rad$ = 1,30 ° +/- 0,49 °, a value which is measured with Photoshop 6.0 considering the theoretical position of the Center of Mass declared in the available technical information (fig E33). Furthermore, the angular velocities ω_0 detected with the previous fits of Figure E31 (for the ascending part) and Figure E32 (for the descending part) are adopted as fixed parameters.

We use the g resulting from the fit presented in Figure E18 in paragraph E.2.1. The results of the fits are shown in Figures E34, E35, E36, and E37. It can be observed that in both cases the proposed model is validated in a very reliable way from a statistical point of view. [*Ann E13*]

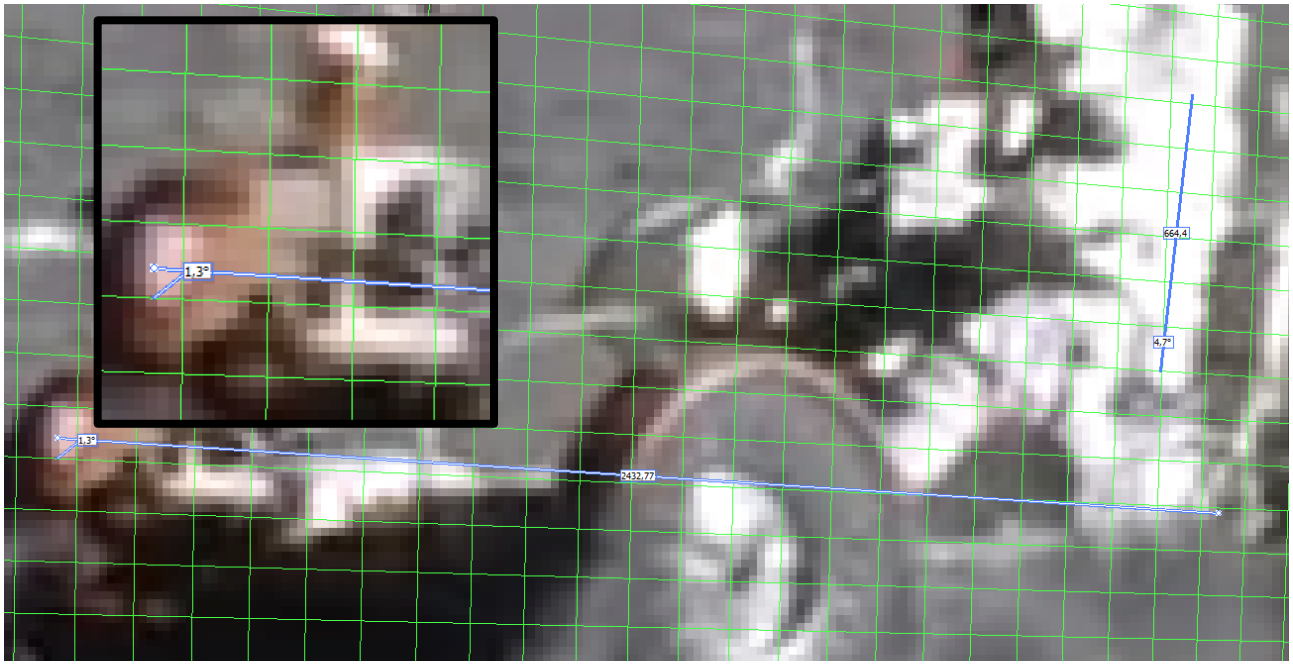

Figure E33 - LRCU Unit - Center of Mass axis tilt at time T_0

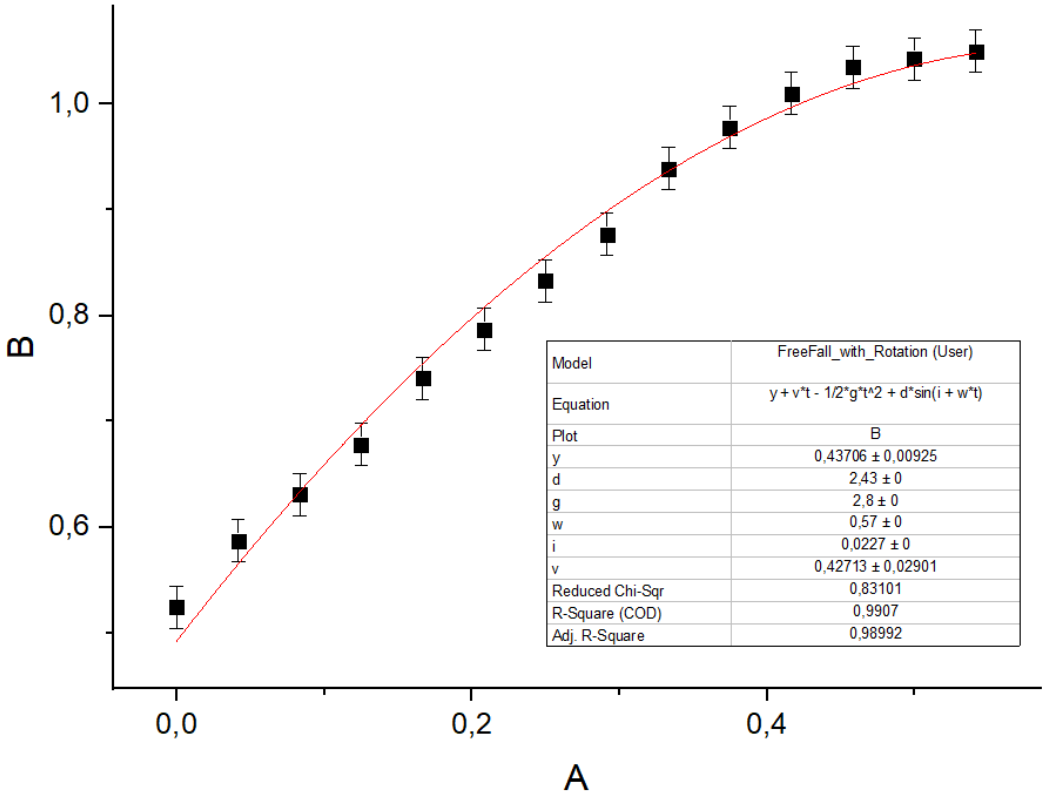

Figure E34 - Free fall and rotational motion of the LRV: fit of the LRCU Unit end tracking from T_0 to T_{13}

Model	FreeFall_with_Rotation (User)
Number of Parameters	6
Number of Derived Parameters	0
Number of Datasets	1
Equation	y + v*t - 1/2*g*t^2 + d*sin(i + w*t)
Report Status	New Analysis Report
Special Input Handling	
Data Filter	No

Input Data

Parameters

		Value	Standard Error	t-Value	Prob>|t|	Dependency
B	y	0,43706	0,00925	47,27379	5,32907E-15	0,72222
	d	2,43	0	--	--	0
	g	2,8	0	--	--	0
	w	0,57	0	--	--	0
	i	0,0227	0	--	--	0
	v	0,42713	0,02901	14,72338	4,8074E-9	0,72222

Reduced Chi-sqr = 0,831013701199
COD(R^2) = 0,99069628894944
Iterations Performed = 3
Total Iterations in Session = 3
Fit converged. Chi-Sqr tolerance value of 1E-9 was reached.
Some parameter values were fixed.
Standard Error was scaled with square root of reduced Chi-Sqr.

Statistics

	B
Number of Points	14
Degrees of Freedom	12
Reduced Chi-Sqr	0,83101
Residual Sum of Squares	9,97216
R-Square (COD)	0,9907
Adj. R-Square	0,98992
Fit Status	Succeeded(100)

Fit Status Code :
100 : Fit converged. Chi-Sqr tolerance value of 1E-9 was reached.

Figure E35 - LRV Free fall: LRCU Unit fit from T_0 to T_{13}, resulting parameters and their reliability

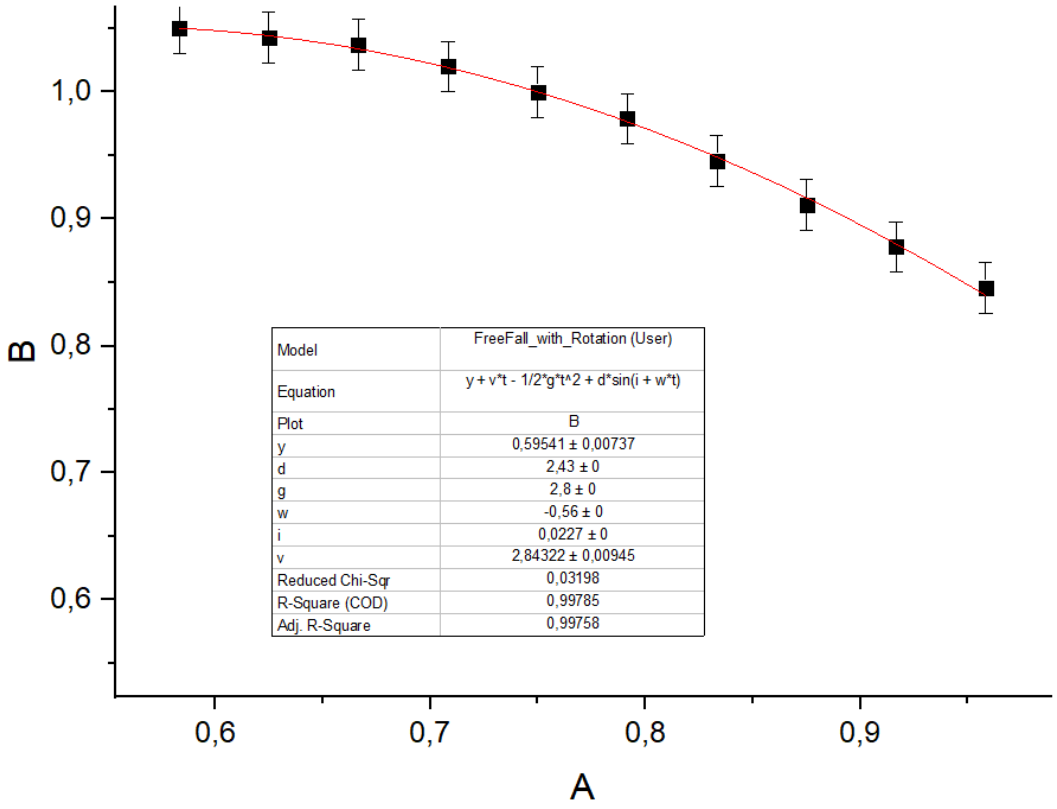

Figure E36 - Free fall and rotational motion of the LRV: fit of the LRCU Unit end tracking from T_{14} to T_{23}

Model	FreeFall_with_Rotation (User)
Number of Parameters	6
Number of Derived Parameters	0
Number of Datasets	1
Equation	y + v*t - 1/2*g*t^2 + d*sin(i + w*t)
Report Status	New Analysis Report
Special Input Handling	
Data Filter	No

Input Data

Parameters

		Value	Standard Error	t-Value	Prob>|t|	Dependency
B	y	0,59541	0,00737	80,76509	6,15952E-13	0,97646
	d	2,43	0	--	--	0
	g	2,8	0	--	--	0
	w	-0,56	0	--	--	0
	i	0,0227	0	--	--	0
	v	2,84322	0,00945	300,85002	0	0,97646

Reduced Chi-sqr = 0,0319813611288
COD(R^2) = 0,99784935998798
Iterations Performed = 4
Total Iterations in Session = 4
Fit converged. Chi-Sqr tolerance value of 1E-9 was reached.
Some parameter values were fixed.
Standard Error was scaled with square root of reduced Chi-Sqr.

Statistics

	B
Number of Points	10
Degrees of Freedom	8
Reduced Chi-Sqr	0,03198
Residual Sum of Squares	0,25585
R-Square (COD)	0,99785
Adj. R-Square	0,99758
Fit Status	Succeeded(100)

Fit Status Code :
100 : Fit converged. Chi-Sqr tolerance value of 1E-9 was reached.

Figure E37 - LRV Free fall: LRCU Unit fit from T_{14} to T_{23}, resulting parameters and their reliability

The effectiveness of the two fits confirms the correctness of the g obtained from the previous study of the Rooster Tails, but it is incompatible with the lunar scenario in which the Grand Prix takes place. If we were to hypothesize an error in the sequence speed, the correct framerate would be:

$$Fr' = Fr * \sqrt{\frac{1{,}62}{2{,}8}} = 24 \text{ fps} * 0{,}76 \approx 18 \text{ fps}$$

However, the Maurer DAC was not designed to run at 18 fps. Furthermore, the images, printed on film and, unlike those of the CTV, did not undergo the long chain of conversions illustrated in the first sections of this study. They were rephotographed many times after 1972 and every film and video sequence produced since then has always maintained the same play speed. It is known that the DAC Camera allowed the use of the following frame rates: 1 fps, 6 fps, 12 fps, 24 fps.

If we consider:

$$g' = \frac{1{,}62}{\left(\frac{Fr'}{Fr}\right)^2}$$

the g values that validate the various usable frame rates in addition to the already proposed value of 24 fps are:

With Fr' = 1 fps then g' ≈ 933 m/s^2
With Fr' = 6 fps then g' ≈ 25,92 m/s^2
With Fr' = 12 fps then g' ≈ 6,48 m/s^2

If among these hypotheses we impose the value of g' closest to the one obtained in E.2.1 (6.48 m/s2) in both the fits of Figure E34 and Figure E35 we obtain a model that is statistically inadequate to interpret the detected data. [*Ann E13*]

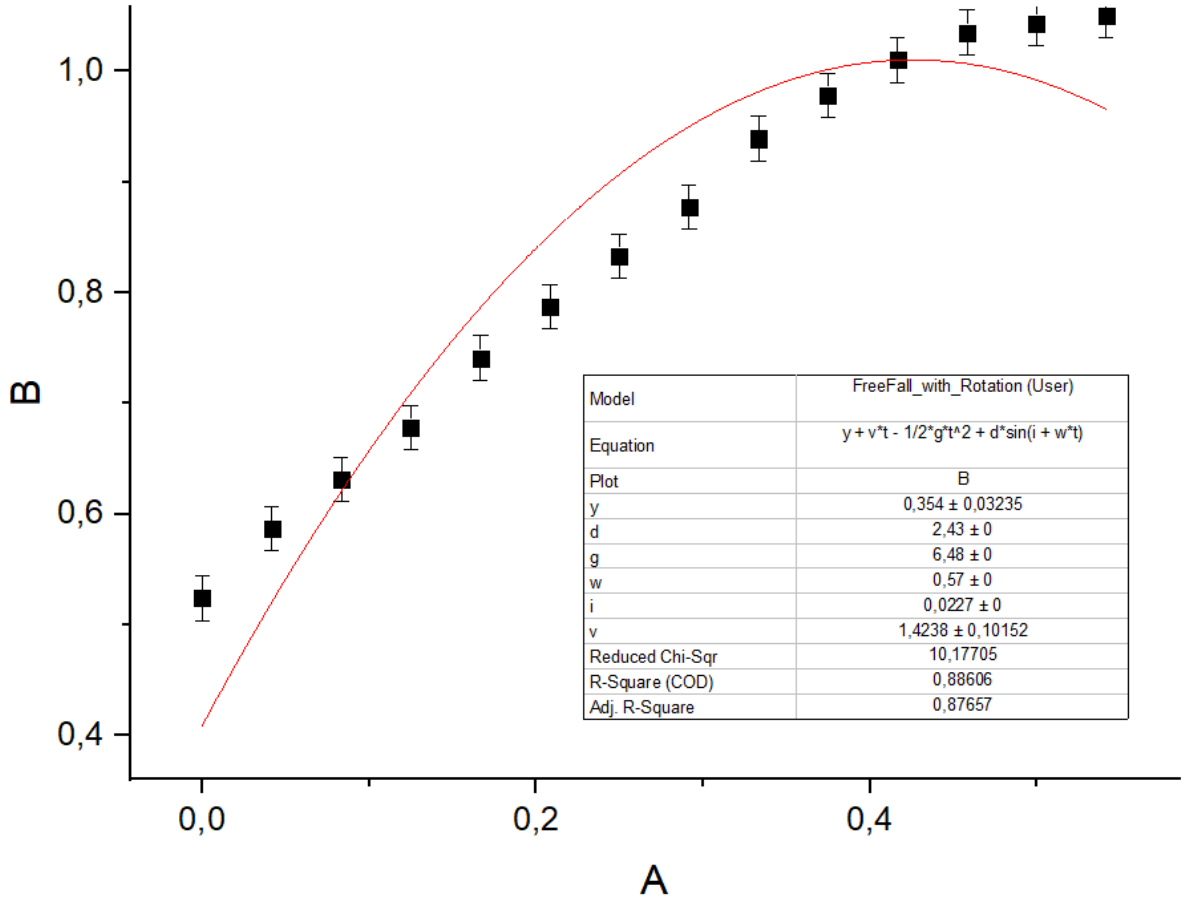

Figure E38 - Free fall and rotation of the LRV: fit of the LRCU Unit from T_0 to T_{13} with a framerate of 12 fps

If we wanted to hypothesize a systemic error in the sizing of the measurements, considering the ratio between g confirmed by the fits in this section (2.80 m/s^2) and expected g' (6.48 m/s^2) with Fr' = 12 fps we would have to hypothesize more than doubled dimensions of the known elements used for the calibration of the system, a hypothesis that we feel we can discard. On the other hand, if the sequence had been filmed on Earth, similarly to what has been hypothesized for other sequences studied in the previous sections, then:

$$Fr' = Fr * \sqrt{\frac{9{,}81}{2{,}8}} = 24 \text{ fps} * 1{,}87 \approx 45 \text{ fps}$$

which is also not a possible option with respect to the frame rates usable by the camera.

There was however another frame rate option in the Maurer DAC Camera, less known than the others. Figure E39 reproduces an example of the Camera. You can see on the upper part of the camera the frame rate selector with 5 positions: starting from the second position the frame rate is explicit, and the first position TIME corresponds to "TIME EXP" ("Time Exposure") as is more fully highlighted in figure E35, which represents the model 290 200 000 of the DAC Camera built in the Gemini missions' era.

Figure E39 – Maurer DAC Camera, framerate selector

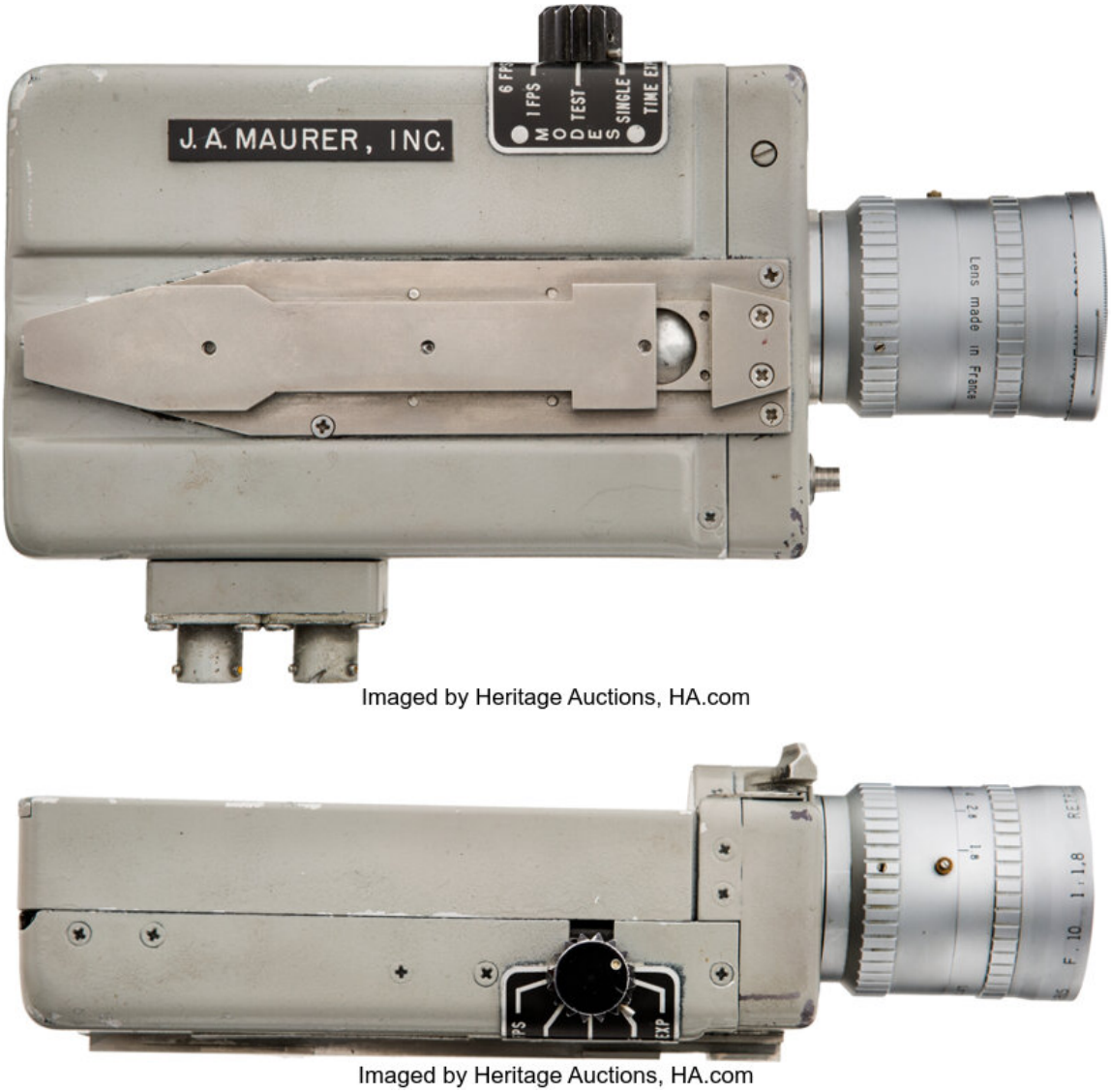

Figure E40 – Maurer DAC Camera, framerate selector [16]

This selector position synchronized the frame rate with the shutter opening when the shutter was set to a speed of 1/60 second. [17] Therefore, although it is not obvious from the markings on the body of the camera, the Maurer DAC was able to record at 60 fps.

Considering the two hypotheses:

---

[16] *https://historical.ha.com/itm/space-exploration/miscellaneous/apollo-moon-missions-prototype-of-the-j-a-maurer-16mm-data-acquisition-camera-with-archive-of-related-photos/a/6139-52051.s Heritage Auctions - The World's Largest Collectibles Auctioneer, 2801 W. Airport Freeway, Dallas, Texas USA.*

[17] *https://www.nasa.gov/wp-content/uploads/static/history/alsj/a11/JSC-07210PltOpsEquip_DAC.pdf Handbook of Pilot Operational Equipment for Manned Space Flight, Report CDHEQA/SL-997, NASA Lyndon B. Johnson Space Center, Houston, Texas, June 1973, page 2.1-4 [Ann E14]*

$$g = \frac{1{,}62}{\left(\frac{60}{24}\right)^2} = 0{,}24\ m/s^2$$

If the scene had been shot on the Moon at 60 fps, the known dimensions at the basis of the calibration of the measurement system should have been reduced by about 12 times (1:12 scale): the LRV would have had a size of no more than 26 cm. This hypothesis should be discarded because, considering what was ascertained in E.1.7, or rather that the Kern lens of the Maurer DAC camera was a 10 mm wide angle, in Frame 2 "Shadow" analyzed in the same paragraph, the camera would be located at only 57 cm from the Rover (see Ann E4) and would have visibly deformed its proportions, but this is not detected.

$$g = \frac{9{,}81}{\left(\frac{60}{24}\right)^2} = 1{,}57\ m/s^2$$

If the sequence had been shot on Earth at 60 fps the known dimensions used for the calibration of the measurement system should be reduced by approximately $\left(\frac{2{,}8}{1{,}57}\right) = 1{,}8$ times, (5:9 scale). Fit with g = 1,57 and with measurements, distance d and speed reduced by a factor of 1.80, would be similar to those shown in Figures E34-E35-E36-E37.

The hypothesis that the sequence was filmed on Earth, on an outdoor set, contrasts with the results obtained in 2.1, since, as we have been able to ascertain, the motion of the roster tails was not affected by the braking effect of the air. Obviously, the experimental results would be compatible with an airless environment such as a large vacuum chamber.

If any errors in our calculations or methodology are identified, we would be grateful for feedback.

If the result of this section will be confirmed during the review and if necessary, by an audit [10], this analysis may suggest that the footage we analyzed should not be accepted as Apollo XVI footage. This statement in no way implies that the Apollo missions did not occur: the effort of the authors of this paper is to protect the scientific truth of the Apollo XVI Mission from counterfeits of any kind and from any source.

About the Authors

Alessio Michelotti (ORCID iD: https://orcid.org/0000-0002-3822-104X)
was born in Lucca (IT) the 31-08-72, and obtained a scientific high school diploma at the Liceo Lorenzini in Pescia in 1991 with a specialization in Physics - Mathematics.
He is a professional researcher in the field of Culture with different publications edited by academic publishers in Italy (like Bulzoni Editore and CUEM).

PhD Andrea Simon (ORCID iD: https://orcid.org/0009-0001-3971-4305)
Headmaster in the "Novalis" Italian Waldorf High School where he is also a mathematics and physics teacher, he obtained his Master's Degree in Physics and his teaching qualification from the University of Padua. Among the most significant previous published works is "*First Results of a Scintillating GEM Detector for 2-D Dosimetry in an Alpha Beam*" edited by IEEE in 2008.

Authors contribution

- Alessio Michelotti: Conceptualization, Data curation, Investigation, Project administration, Visualization, Writing – original draft
- Andrea Simon: Conceptualization, Formal Analysis, Methodology, Software, Supervision, Validation

Conflict of interests

The authors declare that there are no conflicts of interest.

ACKNOWLEDGMENTS

Many people, directly and indirectly, have made this study possible through their collaboration. Most of them have not had the opportunity to see the full content of this work, which may be partly outside their respective research fields. Furthermore, the final results of this paper may not reflect, or be in contradiction with, their beliefs or research. However, we would like to thank each of them for their help and for the effectiveness of their valuable contribution.

We would like to thank for their methodological suggestions and encouragement in research: prof. Luis Bilbao, Universidad de Buenos Aires - Departamento de Física; prof. Andrea Simon, Scuola Superiore Novalis, San Vendemiano (Treviso, Italy); prof. Pasquale Bosso, University of Lethbridge (Canada); prof. Derek Bolton, University of Oxford (United Kingdom); Prof. Franco Macchini, University of Pisa (Italy).

This study would not have been possible without the technical information, scientific support, and documentary materials provided by:

- James T. Hawes, IT Expert technical, writer & editor
- Mark Gray, Spacecraft Films (Atlanta GA), NASA contractor for Video Editing
- Russ Andersson, SynthEyes, Andersson Technologies LLC (Phoenixville, PA)
- Douglas Brown, Open Source Physics (OSP), Davidson College, Davidson NC, USA

English translation by Roberto Leopardi

This study has been reviewed by **Luis Bilbao**, Buenos Aires (ARG); PhD at the Physics University of Buenos Aires; more than 100 publications in international journals; reviewer for the American Journal of Physics and other major scientific journals. Revised sections: Sections B, E.

Their contribution to the review process is documented in a specific appendix (not attached here).

The previous studies "***Analytical Methods for Tracking Bodies Motions on the Lunar Surface in Apollo XVI Footage"*** https://doi.org/10.32388/IA8MXE, ***"Collecting the Big Muley lunar rock sequence of the Apollo XVI Footage"*** https://doi.org/10.32388/COXHKG.2, "***Falling Objects and Dust Particles' Motion in the Collecting Lunar Rock on the Buster Crater sequence of the Apollo XVI Footage***" https://doi.org/10.32388/RFR2D5 have been reviewed as Preprint on the **qeios.com** platform starting from the 22nd April 2024.

The following researchers revised the Preprint sections:

Section 1-3, https://doi.org/10.32388/IA8MXE

- Dr. **Jens Biele German** (h-index 36) Aerospace Center (DLR), Köln (DE) – Astronomy, Geophysics, Experimental Physics and Thermodynamics Researcher. Revised sections: Sections A, B, C.

- Dr. **Alexey Artamonov** (h-index 9), National Research Nuclear University MEPhI - Moscow Engineering Physics Institute, Moscow (RU). Revised sections: Sections A, B, C.

Section 4, https://doi.org/10.32388/COXHKG.2

- Dr. Zhiguo Meng (h-index 18), Jilin University College of Geo-exploration Science and Technology (China)
- Dr. Josep M. Trigo-Rodríguez (h-index 28), Spanish National Research Council, Astrophysics (Spain)
- Dr. Sergey Popel (h-index 34), Head of Laboratory at Space Research Institute, Moscow (Russia Federation)
- Dr. Yanwei Li, Institute of Space Systems, Universität Stuttgart (Germany)
- Dr. Aanuoluwapo Adeloye, Graduate Research and Teaching Assistant, University of Texas at Austin (USA)

Section 5, https://doi.org/10.32388/RFR2D5

- Dr. Aiguo Xing (h-index 18), SJTU · Department of Civil Engineering, Shanghai Jiaotong University (China)
- Dr. Raúl Gutiérrez-Zalapa, Institute of Geophysics and Space Sciences, Universidad Nacional Autónoma de México (México)
- Dr. Stefano Rubino (h-index 21), INAF-IAPS - Istituto di Astrofisica e Planetologia Spaziali, Rome (Italy)
- Dr. P. R. Kumaresan, SRM Institute of Science and Technology, Ramapuram Campus (India)
- Dr. Chonghua Fang, Science and Technology on Electromagnetic Compatibility Laboratory, China Ship Development and Design Center, Wuhan (China)